2019

A Study of Nonlinear Dynamics of EEG Responses to Simulated Unmanned Vehicle Tasks

Ziqing Xu
University of Central Florida

A STUDY OF NONLINEAR DYNAMICS OF EEG RESPONSES TO SIMULATED UNMANNED VEHICLE TASKS

by

ZIQING XU
B.S. China Agricultural University, 2006
M.S.I.E. Auburn University, 2011

A dissertation submitted in partial fulfillment of the requirements
for the degree of Doctor of Philosophy
in the Department of Industrial Engineering and Management Systems
in the College of Engineering and Computer Science
at the University of Central Florida
Orlando, Florida

Spring Term
2019

Major Professor: Waldemar Karwowski

ABSTRACT

In the contemporary world, mental workload becomes higher as technology evolves and task demand becomes overwhelming. The operators of a system are usually required to complete tasks with higher complicity within a shorter period of time. Continuous operation under a high level of mental workload can be a major source of risk and human error, thus put the operator in a hazardous working environment. Therefore, it is necessary to monitor and assess mental workload.

In this study, an unmanned vehicle operation with visual detection tasks was investigated by means of nonlinear analysis of EEG time series. Nonlinear analysis is considered more advantageous compared with traditional power spectrum analysis of EEG. Besides, nonlinear analysis is more capable to capture the nature of EEG data and human performance, which is a process that subjects to constant changes. By examining the nonlinear dynamics of EEG, it is more likely to obtain a deeper understanding of brain activity.

The objective of this study is to investigate the mental workload under different task levels through the examination of brain activity via nonlinear dynamics of EEG time series in simulated unmanned ground vehicle visual detection tasks.

The experiment was conducted by the team lead by Dr. Lauren Reinerman Jones at Institute for Simulation & Training, University of Central Florida. One hundred and fifty subjects participated the experiment to complete four visual detection task scenarios (1) change detection, (2) threat detection task, (3) dual task with different

change detection task rates, and (4) dual task with different threat detection task rates. Their EEG was recorded during performing the tasks at nine EEG channels.

This study develops a massive data processing program to calculate the largest Lyapunov exponent, correlation dimension of the EEG data. This study also develops the program for performing 0-1 test on the EEG data in Python language environment. The result of this study verifies the existence of chaotic dynamics in EEG time series, reveals the change in brain activity as the effect of changing task demand in more detailed level, and obtains new insights from the psychophysiological mental workload measurement used in the preliminary study.

The results of this study verified the existence of the chaotic dynamics in the EEG time series. This study also supported the hypothesis that EEG data exhibits change in the level of nonlinearity corresponding to differed task levels. The nonlinear analysis of EEG time series data is able to discriminate the change in brain activity derived from the changes in task load. All nonlinear dynamics analysis techniques used in this study is able to find the difference of nonlinearity in EEG among task levels, as well as between single task scenario and dual task scenario.

TABLE OF CONTENTS

LIST OF FIGURES

LIST OF TABLES

CHAPTER 1: INTRODUCTION

Mental workload, as defined by Miyake (2002), is the cognitive demand of a task. The growing tendency of mental workload can be witnessed in many a field of contemporary real-world tasks, such as vehicle operations, industrial controls, and military operations, due to the increasing complexity of extensively mentally demanding tasks, the shorter intervals of technological advances, and the short-term yet highly competitive goals of management. The level of mental workload is directly affected by task difficulty. Changes in workload exert remarkable influences on task performance (Kaber et al, 2007). Although operators of a system are usually able to cope with the variation of workloads to keep their performance level, sufficiently high workloads will still make them fail to adapt, and thus exhibit a significant drop in performance (Guastelloet al, 2012, Guastello et al, 2012, Guastello, 2014, Guastello et al, 2014). High mental workload might also cause memory fault (Dunke, 1990). With the increase of mental workload, the function of working memory becomes lower, while the operators exhibit less executive control (Guastelloet al, 2012, Guastello et al, 2012, Guastello, 2014, Guastello et al, 2014). High workload also causes anxiety that might lead to a higher accident rate in the highly hazardous work environment (Guastello, 2015). Task difficulty can also influence the performers' psychophysiological measures. The increasing mental workload can impose various hazards in both systems and operators, such as the increased risks, accident rates, health problems, as well as reduced employee satisfaction, productivity and work performance. Thus, developing more sensitive and

more accurate methods for mental workload measurement has become a crucial matter, especially in monitoring the performance of unmanned systems operations.

Unmanned systems are able to generate relatively high work demand for their operators, for these systems usually requires sudden response to stimuli, urgent processing of a large amount of information, and decision making that has an irreversible consequence, after long periods of low activity. Thus, it is important to establish effective workload measures, in order to obtain better performance prediction. Performance prediction plays a significant role in task design, as well as the selection and training of unmanned system operators. Besides, monitoring and estimation of mental workload are also crucial in the training process, due to training in high workload conditions is more effective and more likely to improve performance.

CHAPTER 2: LITERATURE REVIEW

2.1 Mental Workload

Generally, there are three categories of the tools that are used for measuring mental workload, subjective evaluation, performance measurement, and psychophysiological measurement.

The subjective measures are operators' self-evaluation of workload experience. The major subjective measures include NASA Task Load Index (NASA-TLX), subjective workload assessment technique (SWAT). NASA-TLX considers six subscales namely mental demand, physical demand, temporal demand, own performance, effort, and frustration level. SWAT, on the other hand, measures time load, mental effort load, and psychological stress load.

Subjective measurement is important because people's own perceptions also have a great influence on the workload they experience. For instance, knowledgeable and skilled persons maybe complete a job with minimum effort, but a relatively simple job might create high workload for persons who lack the skill (Rouse et al, 1993).

The performance measures examine mental workload in terms of operators' behavior or performance. The major consideration of performance measures includes task accuracy and the time needed to complete a task. The performance measures and subjective evaluations are usually combined together to estimate relative task efficiency. Task efficiency E can be expressed by $E = (P-R)/2$, where P stands for performance and R refers to mental load. It is considered that the most efficient task has high performance

and low mental effort, and vice versa.

Measurement of reaction time and subjective score are indicators of the variation of the task difficulty. They are more appropriate to be used to indicate memory load and post-hoc measurements instead of continuous indicators of mental load. On the other hand, EEG is an accurate, near real-time, and continuous measurement for mental workload (Zarjam, 2013).

Psychophysiological measures reflect mental workload by means of monitoring the variation of bodily processes and states. This type of measures has the advantage of continuous availability of bodily data and a high level of measurement sensitivity. The commonly used psychophysiological measures include heart rate, respiration rate, blink rate, and electroencephalograph (EEG), among which EEG is accepted as the most reliable method for monitoring mental workload since numerous studies have revealed that high mental workload is closely related to the dynamics of cognitive activity.

2.2 Psychophysiological Effect of Mental Workload

According to the theory of localization theory of brain function, cognitive processing is the result of the simultaneous collaboration of various regions of the brain, and different areas of the brain are assigned for different functionalities. The frontal and central areas of the brain play an important role in attentive tasks. The frontal lobe is responsible for reasoning, emotion, problem solving, and making plans. The parietal lobe is related to movement, feelings, recognition, and perception. The occipital lobe is especially important for visual processing. The temporal lobe is highly related to

memory, speech, as well as recognition and perception of auditory stimuli.

The relationship of mental workload and psychophysiological variations, especially EEG, is well researched. The correlation between mental workload and cognitive activity is well understood. Hong et al (2012) found in a multi-gauge monitoring task that the brain appears to be more active when task difficulty increases. The authors also found relatively higher activity and higher caution level in occipital lobe under the same difficulty level, which is in accordance with the high demand for visual process of the task.

Brooking et al (1996) also studied mental workload using various psychophysiological measures. According to the study, eye blink rate lowered when mental workload increased, which indicated increased demands of visual attention. In the study of Di Stasi (2011) and Cooper et al (2013), mental workload could be tested by means of the change in pupil diameters and the saccadic peak value of eyes. The change in pupillary diameters can reflect the cognitive workload in the process of perceptual tasks, decision making, memory tasks, and complex problem solving (Beatty, 1976).

Respiration rate also increased along with increased task difficulty and mental workload. Carroll et al (1986) also found that respiration rate increased when more difficult laboratory tasks were assigned to subjects. They also found increased heart rate along with the increased respiration rate. Son et al (2011) found that task difficulty could be reflected by the variation of heart rate during a driving task. However, heart rate has limited sensitivity and is insufficient to achieve accurate and reliable measurement of mental

workload (Kaber et al, 2007, Patten, 2007). According to Brooking et al (1996), heart rate was less sensitive than respiration rate because of the a low variation of metabolic demand for different difficulty levels of cognitive tasks. The authors also found that the relative EEG power was sensitive to difficulty levels of the tasks. When task difficulty increased, the theta band activity showed a significant increase in the central area, parietal lobe, right frontal lobe and right temporal lobe of the brain, which inferred more extensive attention demand and memory load. Increased beta activity in frontal and central areas of the brain is also observed as the result of increased processing demands when the brain needed to deal with multi-tasks at the same time. As the difficulty elevated, a drop in alpha activity at temporal lobe was also witnessed. The decrease of alpha relative power with the increase of task difficulty was also observed by Earle and Pikus (1982), Gundel and Wilson (1992). EEG activities in upper alpha band were found related to increasing of mental workload (Mak et al, 2013). In the study by Lei and Roetting (2011) and Hou et al (2015), the increased frontal theta activities and decreasing parietal alpha activities were found related to the increasing mental workloads. The changes in mental workloads had more influence in alpha power. The working memory load, on the other hand, was more associated with the changes in theta power.

EEG is a more reliable method to access the cognitive state of the brain under mental workload, and is analyzed by various statistical and machine learning technique in numerous studies.

Kramer et al (1994) investigated amplitude of N100, N200, and P300 component, which are respectively the mean amplitude of EEG from 75 to 175 milliseconds, from

300 to 400 milliseconds, from 300 to 600 milliseconds post-stimulus, of event-related brain potential (ERP). The subjects performed a simulated radar monitoring task and an oddball task. The results of the oddball task showed that the various stimulus tone type had significant effect on all N100, N200, and P300 ERP. The amplitude of ERP of deviant-attend tone, which subjects attended to deviant other than standard tone, is larger than that of deviant-ignore tone, or standard tone. The analysis of radar monitoring task showed that the amplitude of ERP decreased significantly as the task level changed from base-line to low-load condition and then to high-load condition for all N100, N200, and P300 components. The study also found that ERP at EEG channel Fz was sensitive to changes in workload.

Ullsperger et al (2000) also studied the physiological effect of mental workload for a gauge monitoring task, a mental arithmetic task, and a dual task. N100 and P300 component of ERP were analyzed for 30 EEG electrodes. The result of this study showed that ERP was able to distinguish the increase of the level of brain activity in the following brain areas as the task difficulty increased, the task performance declined, and the overall workload and temporal demand increased. First, the areas related to perceptual, central and spatial perception and manual output for the gauge monitoring tasks. Secondly, the areas related to visual input, speech output, and working memory for the mental arithmetic task. Thirdly, the areas of perceptual and central stages of processing for the dual task.

Brookings et al (1996) studied the effect of mental workload in two scenarios with three difficulty levels on the computer simulated terminal radar approach control

(TRACON) task. The subjective measures NASA TLX was recorded. The physiological measures included heart rate, eye blink rate, saccade rate, and amplitude, respiration rate and amplitude, and EEG. As the task difficulty increased, NASA TLX score and blink rate declined, whereas respiration rate and heart rate increased. However, these measures could not reflect the change of traffic manipulation types. On the other hand, EEG data was sensitive to various difficulty levels. Theta power and beta power both increased in frontal and temporal lobe in right hemisphere, as well as in the midline central sulcus and parietal lobe. Alpha power decreased while difficulty increased. Alpha power and delta power were also demonstrated to be sensitive to the interactions of difficulty and traffic manipulation types. In this study, EEG is the only mental workload measure that was able to reflex changes in traffic type differences.

In the study presented by Zhong and Zhang (2014), the authors introduced a new approach to estimate the relation between EEG and mental workload. The modeling techniques, namely locally linear embedding (LLE), support vector clustering (SVC), and support vector data description (SVDD) were used in order to classify the change of mental workload based on EEG data. The LLE was used to produce the mental workload indicators. The SVC approach was applied to elicit clusters of the mental workload indicators in order to detect the variation of mental workload. At last, the SVDD was used as a classifier that could detect more delicate changes in the mental workload indicators. In this study, the computer-based simulated task was for human operators to remotely monitor and repair the systems in spacecraft from earth with different task difficulty. The result of the study was able to discriminate the ten task

scenarios as three mental workload, namely low, normal, and high levels by means of computing the identification accuracy using different combination of the three proposed models.

In the study of Berka et al (2007), different linear and non-linear classifier models were used in order to investigate the correlation between EEG and mental workload in memory tasks. The authors defined EEG engagement as the result of the calculation of a four-class quadratic discriminant function analysis (DFA) based on the EEG absolute and relative power spectral density. The workload classifier was constructed by means of linear DFA with two categories, namely high and low mental workload. The study succeeded in detecting the decreased EEG engagement level in corresponding to decreased task performance and increased reaction time and task difficulty. The study found that for the learning and memory tasks, the EEG-engagement model was able to distinguish the changes in task difficulty, particularly during of encoding and recognition period of the memorizing process. The result of the study indicated that EEG was able to reflect the allocation of attention resources and variations of mental workload when encoding memory.

Humphrey and Kramer (1994) employed bootstrapping analysis of ERP for computation of level of accuracy for differentiating mental workload levels. The bootstrapping analysis was an iterative sampling technique in which the amount of averaged ERP data was systematically incremented and finally classified into two mental workload levels. The classifying method employed in this study was linear stepwise discriminant analysis. In this study, the task included a gauge-monitoring task

with two task conditions, a repetitive arithmetic task with two difficulty levels. EEG was measured at midline electrodes, Fz, Cz, and Pz. P300 ERP was measured at electrode Pz. Using this approach, P300 ERP was able to discriminate the difference between the single task and dual task condition. The algorithm that was used in this study achieved 90% accuracy for classification of mental workload levels.

Similarly, in the study of Humphrey et al (1990), the bootstrapping analysis was performed on the ERP derived from a gauge-monitoring task and an arithmetic task. The ERP component that was analyzed in this study included 1) base-to-peak measures of P300 amplitude (P3bp), the largest positive value in the waveform between from 300 to 800 milliseconds post-stimulus. 2) Measures of P300 area (P3area). 3) Cross-correlation measures of P300 amplitude (P3cross), calculated by moving a 300-millisecond wide cosine wave across the P300 period. 4) Area measures of a late slow wave component (SWarea), the area between 750 and 1,100 milliseconds post-stimulus. The study found an inverse correlation between accuracy and levels of task difficulty for both the gauge-monitoring task and the arithmetic task.

Miller et al (2010) investigated the relationship between N1, P2, P3, late positive potential (LPP) component of ERP at midline electrodes, Fz, Cz, and Pz, and the task difficulty. The result of the study suggested that for the component N1 at Cz electrode, P2 at all electrodes, P3 and LPP at Pz electrode, ERP amplitude decreased as the difficulty level was higher. The study also concluded thatP3 and LPP were more sensitive to variations of mental workload than components N1 and P2.

Wilson (2002) studied the mental workload derived from aircraft flight tasks. The

subjects, who were experienced pilots, were required to complete a total of twenty two simulated flight tasks during the experiment. The result of this study suggested that the alpha power of EEG in parietal lobe reduced for the tasks with higher complexity such as takeoff and landing. As the task difficulty increased, higher delta power in central and right parietal scalp was observed. The significant decline in beta power was also observed in the tasks with higher difficulty, but was rarely seen in the tasks that had less cognitive demand.

Sirevaag et al (1993) also examined the mental workload of experienced pilots produced by different communication formats, in terms of information magnitude and input types, in a simulated helicopter flight task. The P300 component of ERP at midline electrodes was also used as the physiological measure in this research. The study concluded that the larger P300 amplitudes reflected the decrease in processing demand for low communication load. On the other hand, the subjective measures used in this study, NASA TLX in this case, failed to indicate the changes derived from the rising of communication load or the changing of communication format.

Borghini et al (2012) estimated the occurrence of diver's mental fatigue by detecting EEG alpha band spindles. The study employed a monotonous driving task to measure drive's alert and vigilance. The result of the study revealed that the appearance of alpha spindles, defined as the short bust in EEG alpha band amplitude, was a sign of the occurrence of drowsiness during driving car, and was consistent with driving errors. The study defined the mental workload indexes as the ratio of theta power spectral density in frontal areas to alpha power spectral density in the parietal areas, for the left

side, the midline, and the right side of the brain respectively. The study also concluded that the higher workload index was in consistency with higher task difficulty and increase of vigilance task errors and driving errors.

Chaouachi et al (2011) characterized mental workload by means of spectral analysis of EEG. The participants were required to solve trigonometry problems in the experiment. The study recorded participants' EEG data and employed Fast-Fourier Transform to transform EEG data into power spectral density. The authors calculated the correlations among pretest scenarios, in which the participants only answered basic concept questions, learning period, and six problem solving task scenarios with gradually increasing task difficulty level. As the result of the study, significant increase of EEG power spectral density was found between the learning period and the pretest condition, the task level 4, 5, and 6, with the highest difficulty levels, and the pretest condition, the task level 5 and 6 and the first four level of tasks. The study computed the bi-variate correlation between EEG power spectral density and the response time. The significantly positive relationship between workload level derived from EEG analysis and the difficulty of problems. The by-variate correlation results validated the significant linear relationship for different task levels and the time spent on problem solving. The bi-variate correlation was also calculated between EEG power spectral density and task performance. However, the significant linear relationship was only found in the pretest condition.

In the study conducted by Brouwer et al (2012), EEG spectral power and ERP were employed as objective measure of mental workload in the n-back memory tasks.

The result of this study revealed that the variation in alpha band power was able to distinguish the change of task levels, for example from a 0-back task condition to a 2-back task condition. The alpha band power decreased when memory load became higher at midline EEG locations. For ERP analysis, the decreased P300amplitude was observed in 2-back task condition compared to 0-back task condition at midline parietal areas. The study also concluded, by computing classification accuracy, that combining both power spectral analysis and ERP analysis, with 88% accuracy, could improve the estimation of mental workload, compared with using each of the methods alone, especially when data size was not large enough.

Gundel and Wilson (1992) investigated the interrelationship between mental workload and topographical distribution of EEG. The study used randomized block factorial design for statistical analysis of EEG, in which experimental condition, EEG frequency band, and element of the broadband crosspower matrix served as three factors. The broadband crosspowers were the result of the logarithmic transformation of the averages of the absolute values of spectral matrix elements in certain EEG frequency band. The cognitive tasks in the experiment were presented with two different difficulty levels. For the visual tasks, the reduction of alpha band power was found in parietal and occipital lobe for the higher difficulty level. The change in theta band power was concluded insignificant across the difficulty levels in this study. However, a trend of increase was found for the higher difficulty level in left frontotemporal areas. For the auditory task, an increase in theta power band power was observed in left frontal areas.

Trejo et al EEG (2007) estimated the alert and fatigue states in mental arithmetic tasks. EEG was classified using two models. The first model was kernel partial least squares (KPLS) decomposition with a discrete-output linear regression classifier. A score was given for each randomly separated EEG segment. The KPLS component scores were analyzed by means of Bayesian optimal data-based binning methods. The second model used in this study was an autoregressive model for each EEG channel and EEG epoch. The score of the models was able to categorize the EEG into three states, namely heightened alertness, normal alertness, and fatigue. Furthermore, the models were also able to detect the change of states for the EEG segments within the time series.

In the study of Lim et al (2015), the classification of EEG power spectral density was performed for 4 classes and 2 classes in order to compare the accuracy between classifiers for mental workload. EEG data was recorded for three types of tasks, a visual match task, an auditory based problem solving task, and a dual task that combines the two tasks, with four successive difficulty levels. The classification accuracy of EEG power spectral density was calculated, and was subsequently validated by means of Support Vector Machine (SVM) and k Nearest Neighbors (k-NN), as long as other analysis methods such as statistical analysis, Higuchi Fractal Dimension (FD), wavelet entropy, and event related potentials (ERP). The highest classification accuracy for the SVM classifier was achieved by means of the combination of statistical analysis and FD, with 80.09% for 4 classes and 90.39% for 2 classes. SVM classifier achieved a higher classification accuracy than k-NN. The study succeeded in distinguishing

different mental workload levels using EEG data. The larger the difference of difficulty levels between two tasks, the higher classification accuracy was obtained.

Kathner et al (2014) evaluated the mental workload in dichotic listening tasks with two difficulty levels using P300 amplitude of ERP. The result of the study also confirmed that the overall ERP reduced when the mental workload increased. For this experiment, the variations of workload had no significant effect on alpha band and the theta band at midline parietal lobe between two tasks levels. However, declined alpha band power and significantly increased theta band power in fronto-central locations was found in the screening run compared to the low or high task level. The alpha power was heightened in parietal and parieto-occipital areas. The study also found the increased alpha power in the last task trials compared to the first trials.

Gevins et al (1998) examined the effect of a memory task among three cognitive load on the EEG pattern. The authors used neural network based pattern recognition method with the Joseph-Viglione algorithm to assess EEG data. The power spectral analysis indicated alpha power was larger for verbal tasks compared to the spatial tasks, and was largest in parietal-temporal-occipital areas. Beta power was at its peak in midline central areas. Theta power was largest at midline frontal lobe. The neural network based classification succeeded in distinguishing the change of memory load between task levels and EEG locations. The result of the study revealed that, in the memory tasks, alpha power was most frequently weighted in parietal and occipital lobe, theta power was less frequently weighted, and beta power had relatively scarce contribution.

Sammer et al (2007) assessed the mental workload derived from a mental arithmetic task with sixteen trials. The power spectral density of EEG was analyzed in this study. The significant increase of theta power was obtained from the task performing condition with the baseline condition. The higher amplitude of theta power was found in frontal locations. On the contrary, the task had no significant effect on alpha power. Additionally, alpha power was higher in the posterior brain areas than in the frontal lobe. Theta power was higher at the first mental arithmetic trials and declined in the later trials. This reduced theta power was still larger than the baseline condition.

2.3 Nonlinear Dynamics of EEG time series

2.3.1 Nonlinearity in EEG Time Series

Nonlinear dynamics is a theory that considers the structure as well as the amplitude of the variability of the systems. It looks deep into the underlying process that creates the variability and affects the system outcomes. The temporal patterns are one of the typical examples of nonlinear dynamics. The nonlinear dynamics was applied to ergonomic as early as the 1980s. Its early application ranges from the study of shift work and industrial production as well as the study of physical workload, fatigue, and occupational hazards. Nowadays, its application has branched out into the field of psychology, including neuroscience, perception, cognition, sensation, and so forth. The nonlinear dynamics expand the understanding of cognitive workload and fatigue, provides answers to the questions that cannot be solved before. It is now understood

that nonlinear dynamics is a significant causal factor for the change in human performance (Guastello, 2001, Guastello, 2016).

The underlying process of human behavior is not as stable as the laws of physics (Sterman, 1987). The complex human responses can reflect nonlinear properties, in which the slight changes in the initial task conditions induce remarkable changes in human performance for both cognitive and physical tasks over a period of time. The process of human system interaction is sensitive to initial conditions and might give rise to chaotic behaviors. Hence, nonlinear dynamics is especially suitable to be applied to the examination of the variability in human performance among repetitions of certain task (Karwowski, 2012). Thus, it is important to apply the theory of nonlinear dynamics in order to enhance performance and match human capacities and limitations to predict the task outcome (Karwowski, 2005). In many a contemporary work systems, human performance is subject to the sensitivities to the initial conditions and therefore can be reflected by chaotic behaviors (Karwowski, 2009). Nonlinear dynamics was used to examine the temporal dynamics of the performance of emergency response team, in regarding with their self-organization and coordination process (Guastello 2010).

The multivariate property of the EEG time series is the result of the simultaneous electrical activity of a massive amount of neurons. The EEG signals are the superposition of random waves of electric discharge that passes through the network of countless neurons. Therefore, the EEG recording shows great complexity that develops in time. Due to the complex nature of the EEG records, the time-frequency analysis, which relies on linear approaches, is not adequate to discover the subtle changes and

significant properties hidden in the time series. Besides the cellular level non-linearity, the evidence that the brain is able to accomplish complicated cognitive tasks also disproves the hypothesis that the brain activity is a stochastic process. Hence, the nonlinear dynamics, based on the deterministic chaos theory, is more suitable for analyzing EEG data. Since the introduction of the nonlinear dynamics, deeper and more important information about the brain activities has been obtained from the interpretation of EEG data. The nonlinear dynamics makes it possible to apply EEG data in various fields of clinical research in order to gain more useful insight regarding how the brain works.

2.3.2 Deterministic Chaos

Deterministic chaos is referred to a phenomenon that the variables of a system are able to generate irregular fluctuations. The primary characteristic of chaotic behaviors is the sensitivity of the system depending on the initial values. The outcome of the system can be extensively different if its initial condition slightly changes. In contrast with randomness which usually features infinite degrees of freedom, deterministic chaos tends to be produced from a finite or even a small number of degrees of freedom. The quantifiers of chaotic behaviors have been proved to be able to reflect the changes in cognitive behavior and the mental state of the brain. Therefore these behaviors require techniques that are superior to the traditional research methodologies used in cognitive ergonomics (Karwowski, 2000). For example, the

variation of work motivation exhibit chaotic behavior within human behavior, obtained from the calculation of Lyapunov exponents, self-recorded motivation index time series (Navarro and Arrieta, 2010).

The primary traditional mathematical measures of chaos include correlation dimension, maximal Lyapunov exponent, Hurst exponent, and entropy. Correlation dimension (Grassberger and Procaccia, 1983) characterizes the number of dimensions in phase space that are required to define an attractor. A lower correlation dimension corresponds to a more regular system, lack of complexity. On the other hand, a higher dimension represents a more complex system, which is associated with growing awareness and more frequent cognitive activity. A positive Lyapunov exponent is a sign of chaotic behaviors in the system, indicating the existence of complex brain activity (Wolf et al, 1985). The larger value and the more occurrence of positive Lyapunov exponent suggest the existence of a more complex behavior. Entropy describes the two points in the phase space of the embedded time series that are close to each other but separated in time (Kannathal et al, 2005). It is an indicator of the predictability of a part of the trajectory relying on another part. Higher entropy is a sign of less predictability and stochasticity. On the other hand, lower entropy indicates regular dynamics. Hurst exponent measures the non-stationary behavior of the time series (Kannathal et al, 2005). The higher value of Hurst exponent indicates less complexity in the system and vice versa.

In the study of Kannathal et al (2005), the values of the correlation dimension of the actual EEG data differed by more than 50% to that of the surrogate data which

generated from the same EEG data. This result mathematically testified the non-linearity that resided in the EEG time series. In this study, the correlation dimension that was calculated from the EEG segment during the epileptic seizure was less than that from the EEG segment when seizure was absent. The lower dimensionality during seizure indicated less brain activity. Moreover, the distinction between epileptic and healthy EEG data was supported by means of statistical analysis using t-test with p-value less than 0.0001. The reduced maximal Lyapunov exponent, the increasing Hurst exponent, and the decreasing entropy were also observed during the seizure. All the mathematical methods agreed each other and resulted in the same conclusion that less chaotic behavior in the time series indicated less neural process in the brain.

In this study, the mathematic methods were tested again using alcoholic EEG compared to normal EEG. The same results were obtained. The decreased results of the correlation dimension, the maximal Lyapunov exponent, and the entropy, as well as the increase in the Hurst exponent were observed in the alcoholic EEG. The difference between two datasets was statistic significant with the p-value less than 0.0001.

Quiroga (1998) also reviewed some traditional methods of nonlinear dynamics that were used to interpret EEG data. In this study, the maximal Lyapunov exponent methods had succeeded to detect the chaos that was omitted by the very low correlation dimensions, during an epileptic seizure. The maximal Lyapunov exponent was also able to detect more arousal brain activity in the state II sleep compared to the deeper stage IV sleep, by providing a higher value for the former. The positive values of Lyapunov exponent were found in all four stages sleep and REM sleep, which disproved the

statement that there was only meaningless noise in EEG recording during sleep. The drop of the maximal Lyapunov exponent during seizures was witnessed in the author's study. The similar result was obtained for the correlation dimension as well, leading to the conclusion that more regular dynamics was found during the seizures.

In the study conducted by Kar et al (2010), the EEG recordings were analyzed using entropy methods in order to develop a quantitative way for measuring mental fatigue. The subjects were required to complete both actual driving tasks and simulated driving tasks in the state of sleep. The 3-minute long EEG time series were acquired. Five types of entropies were calculated in this study, namely Shannon's entropy, Rényi entropy of order 2 and 3, Tsallis wavelet entropy and Generalized Escort-Tsallis entropy. The increasing entropy values were found with the accumulation of driving time. This increasing trend of entropy values were also in accordance with the increase of subjective fatigue levels reported by the subjects.

In the study conducted by Liu et al (2010), EEG data was analyzed using approximate entropy and Kolmogorov complexity were used to detect mental fatigue after cognitive task. The significant decrease, where p-value was lower than 0.05, was observed for both approximate entropy and Kolmogorov complexity values when subjects finished various cognitive tasks after they felt exhausted and quitted. During the tasks when the entropy values were higher, the rhythm of EEG was with high frequency and low amplitude, indicating the state of desynchronization and high level of brain activity. After the subjects gave in with exhaustion, the rhythm of EEG switched to a state of synchronization which featured low frequency and high amplitude,

indicating the uniformed pace of electric activity of neurons in brain cortex and low level of brain activity. The changes in approximate entropy clearly detected this change in the level of brain activity.

Azarnoosh et al (2011) also tried to detect mental fatigue utilizing nonlinear dynamics of EEG signals. The mathematics method they applied was Shannon's entropy. In the experiment, they used a long-term attentive task in four consecutive trails in order to product mental fatigue for the subjects. By calculation and comparison of entropy values of EEG recordings in different trails, the entropy value was higher in the first trial than in the last trail when the mental fatigue occurred. The authors concluded that the brain activity level was high in the commencement trail because that attention required more neural stimulations. After undertaking long periods of attentive tasks, the fatigue had made the activity of the brain reduced. Entropy increased with higher attentive state of the brain, and decreases with long-term fatigue. In other words, the decreased entropy could be treated as a signature of decreased brain activity.

Murata and Iwase (1998) investigated the EEG time series using fractal dimension. EEG data was recorded when subjects worked on arithmetic tasks which consisted of addition of two numbers with four difficulty levels. The largest Lyapunov exponent calculated from frontal lobe and central lobe was all positive for all work levels, indicating the existence of chaotic behaviors. The authors calculated the fractal dimension using the method by Grassberger and Poincare (1983). Fractal dimension increases with the increasing work difficulty levels. As a result, fractal dimension was proved successful to indicate cognitive work demand and mental workload.

In the study conducted by Lutzenberger (1992), the fractal dimension of EEG time series, which were recorded when subjects were asked to complete a series of tactile and imagery tasks, were calculated and compared. The result showed that the fractal dimension decreased for alpha activity in the tactile and the visual attention tasks, and increased for alpha activity in the imagery tasks, which indicated a higher brain complexity for internal processing than for perceptual processing. Besides, these significant differences all occurred in frontal lobe, which was in accordance with the higher activity level of frontal lobe during the thinking process. The authors also pointed out that such information was not found in their previous studies with the same data using conventional power estimation of EEG bands.

According to the study conducted by Miao (2012), the changes in chaotic behaviors of EEG time series were measured by means of computing the largest Lyapunov exponent using improved Rosenstein algorithm. The extensive increase of largest Lyapunov exponents was found in occipital lobe and right cerebral area when subjects performed speaking tasks. On the other hand, the largest Lyapunov exponents reduced when subjects were listening to peaceful music. The study concluded that the increase in chaotic behaviors of EEG time series was a useful demonstration of the increase in brain cognitive activity. Besides, this change was able to be reflected by the increase of the largest Lyapunov exponent values.

There is much more evidence. The progress of brain development was observed by examining the changes of Lyapunov coefficients in frontal brain areas among different ages, which was used as an evidence of the maturation process of the brain (Meyer-

Lindenberg, 1996). The evidence of the existence of chaos in EEG recording was found by computation of Lyapunov exponent and correlation dimension (Wand and Luo, 2006). The study has also revealed the changing chaotic behavior of EEG responded to different emotions within the posterior temporal areas of the brain. Negative emotions tended to generate more bounded and normal dynamics, whereas the positive emotions tended to produce greater chaotic behaviors, indicating greater complexity and activation of the neural networks. The nonlinear dynamics can access more sensitive change in EEG data than power analysis of EEG. It can detect the variation related to emotional change that cannot be revealed by linear analysis (Aftanas et al, 1998). Studies have found the variation process of attention during physical effort by means of nonlinear analysis of the using nonlinear dynamics (Balague et al, 2012). By examining the Hurst exponent, research also found that nonlinear dynamics is more predictable when brain is more activated with increasing task difficulty and vise versa (Diaz et al, 2015). Using the technique of phase space reconstruction, the shapes of attractors of EEG time series showed significant change under various mental workload levels (Tumey et al, 1991). By nonlinear analysis of EEG time series, it has been succeeded in identifying frontal and occipital lobe as the influenced regions during arithmetic tasks. The study revealed that the correlation dimension increased, the Hurst exponent and approximate entropy declined while the task difficulty rose, as the EEG showed more regular behaviors (Zarjam et al, 2012). The study indicated that the imagery process required more complex brain activities than perception of an actual object, with higher fractal dimension (Lutzenberger et al, 1992). The more intelligent a

person is, his or her brain has more complex nonlinear dynamics, higher dimensional complexity, while resting, might derive from self-initiated cognitive behavior (Lutzenberger et al, 1992).

Natarajan et al (2004) employed nonlinear measures including correlation dimension, Lyapunov exponent, Hurst exponent, and approximate entropy to investigate the difference of complexity of EEG recorded from resting condition, listening to music, and under gentle foot reflexologic stimulation. The result of the chaos quantifiers found reduced nonlinear complexity and randomness in EEG when subjects were under the influence of music and reflexologic stimulus, suggesting the state mind change into a more relaxed state compared with the resting condition. The increased Hurst exponent, declined correlation dimension, largest Lyapunov exponent, and approximate entropy were obtained from the computation, evidently demonstrated the reduction of randomness in EEG time series.

Iasemidis and Sackellares (1996) found that the change in complexity of EEG was related to the onset of epilepsy seizures. The study recorded the EEG from subdural and depth electrodes for the before seizures preictal, during seizures ictal, and after seizures postictal states. The authors stated that occurrence of epileptic seizures could be represented by the phase transitions of the chaotic characteristics of EEG. Distinct difference of the value of Lyapunov exponent was found among the three states. The largest Lyapunov exponent was largest in postictal state, lower in preictal state, and lowest in ictal state. The discharge of epileptic seizure less complex state. As the result of nonlinear dynamic analysis, several minutes before the occurrence of temporal

lobe epilepsy seizure, the change of the largest Lyapunov exponent happened in anterior temporal cortex. Subsequently, the change of the largest Lyapunov exponent was detected in locations distant from the onset, later in hippocampal depth electrodes, demonstrating the pattern of the change in chaotic characteristics happened in EEG.

Before investigation of physiological nature of the epileptic seizures was often achieved by visual inspection or traditional signal processing techniques of EEG. However, more subtle changes in brain cannot be obtained from visual inspection of EEG, such as the change of nonlinearity in hippocampal depth EEG. Less random behavior in interictal and preictal states was observed than the contralateral hippocampal EEG in normal state. Moreover, by detecting the change of complexity in the brain several minutes before seizure onset, prediction of the epileptic seizures becomes possible.

2.4 Nonlinear Dynamic Analysis Methods

2.4.1 Fractal Dimension

Correlation dimension is an important and a widely used technique for mathematically determining the fractal dimension of chaotic time series. Its algorithm, as proposed by Grassberger and Procaccia (1983), measures the complexity of the system that is relative to its degrees of freedom. The first step of calculating the correlation dimension is to construct a phase space, in which the evolution of a system through time is represented (Prichard and Duke, 1995). The “time shift method”

(Takens, 1981) is used to reconstruct the space phase, using the following formula, in which m is the embedding dimension, τ is the time delay, and the vector $\vec{x}$ is a point in the phase space which represent a state in the system.

$$\vec{x} = \{x(t), x(t+\tau), \dots, x(t+(m-1)\cdot\tau)\} \quad (1)$$

Then the correlation integral C(r) is calculated. C(r) is the probability that two arbitrary points in the phase space that has distance smaller than r, where the vector $\vec{\mathrm{x}}$ is the point in the phase space, and θ is theHeaviside function.

$$\mathrm{C(r)} = \lim_{\mathrm{N}\to\infty} \frac{1}{\mathrm{N}^2} \sum_{\mathrm{i}\neq\mathrm{j}} \theta(\mathrm{r} - |\vec{\mathrm{x}}_\mathrm{i} - \vec{\mathrm{x}}_\mathrm{j}|) \quad (2)$$

Then, correlation dimension is calculated.

$$\mathrm{CD} = \lim_{\mathrm{r}\to 0} \frac{\log(\mathrm{C(r)})}{\log(\mathrm{r})} \quad (3)$$

2.4.2 Lyapunov Exponent

Lyapunov exponent (λ) quantitatively measures the level of chaos in a system. It indicates the sensitivity of the system depending on the initial conditions. It determines the average rate of divergence of two trajectories with time. More rapid diverges of the neighboring trajectories imply that the system is more chaotic and is more sensitive to initial conditions. A negative exponent indicates that the trajectories are approaching a common fixed point. A zero exponent implies that the trajectories are maintaining the relative positions and are on a stable attractor. A positive exponent means that the trajectories are on a chaotic

attractor.

Using the algorithm proposed by Wolf et al (1985), the first step to calculate Lyapunov exponents is the phase space reconstruction. For the time series $x(t)$ in the phase space with *m* embedding dimensions and delay coordinate *t*, $\{x(t), x(t+t), \dots, x(t+(m-1)t\}$, the nearest neighbor to the initial point $\{x(t_0), x(t_0+t), \dots, x(t_0+(m-1)t\}$ is located. Given the distance (L) of t these two points, after the system evolves for a period of time, the length between these two points will change to a new distance (L′). Then repeat the evolution process and calculate the successive distances until the divergence is larger than the threshold. The average exponential rate of divergence of two initially close trajectories is calculated using the formula:

$$\lambda = \frac{1}{t_M - t_0} \sum_{k=1}^{M} \log_2 \frac{L'(t_k)}{L'(t_{k-1})} \tag{4}$$

The embedding dimension, the time delay and the evolution time must be selected.

2.4.3 Entropy

Entropy measures the rate of information loss for dimension of the attractor and indicates the amount of disorder in the system. Entropy is derived from the embedded time series by finding points that are close in phase space but separate in time. The velocity of these points move away from each other is observed. The time that these points take to move away from each other can be represented by

Kolmogorov entropy (K). The Kolmogorov entropy can be calculated using the formula $\langle t_{div} \rangle = 2^{-Kt}$, where $\langle t_{div} \rangle$ is the time for divergence. The higher Kolmogorov entropy reflects the less predictable and more stochastic the system (Kannathal et al, 2005).

Kolmogorov entropy can also be expressed by the sum of the positive Lyapunov exponents, with the following formula. (Quiroga, 1998)

$$K_2 = \sum_{\lambda>0} \lambda_i \tag{5}$$

2.4.4 Hurst Exponent

Hurst exponent is another way for estimating the fractal dimension. It is often used to characterize the smoothness or the roughness of the time series. Hurst exponent indicates the strength of the dependence of the time series to its own past histories. Its H parameter has values ranging from 0 to 1, with the value 0.5 serving as a phase switching boundary. With H between 0 and 0.5, the system is more unpredictable, suggesting long term shifting in sequential values. When H is between 0.5 and 1, the system is considered to be steady and does not have drastic change. Whereas the value 0.5 suggests that the time series is subject to uncorrelated Gaussian noise. The Hurst exponent is an indicator of the rate of chaos (Diaz et al, 2015). The Hurst exponent can detect fractal random time series. The relationship between Hurst exponent and fractal dimension (D) is $D = 2 - H$.

2.5 0-1 Test for Chaos

The 0-1 test was proposed by Gottwald and Melbourne (2003) as a new test to examine chaotic behaviors.

The data input of the analysis is the observables that come directly from the measurement. Thus, the 0-1 test has the features of universality, as well as the independence of the data, which indicates that almost any measurement data could be applied to this test method. The method is irrelevant to the underlying equations of the system. It has the advantage of suiting the system of which the knowledge of the underlying dynamics is unknown. Thus, it is an extraordinary option for analyzing EEG time series.

Besides, unlike traditional methods, such as computing Lyapunov exponent, which require phase space reconstruction, 0-1 test doesn't have limitation of dimensions. Large embedding dimensions will result in smaller maximal Lyapunov exponent, causing ambiguity of the result. As a result, the high dimensionality of the attractor requires the time series to be sufficient in length to allow asymptotic Brownian behavior to occur and that data becomes stationary and deterministic.

2.5.1 Algorithm of The 0-1 Test

The original data will be transferred into a set of translation variables p(n). The test assumptions include that p(n) is unbounded and presents diffusive behavior

resembling Brownian motion if the underlying dynamics of the system is considered to be chaotic.

After p(n) is determined, the mean square displacement is calculated in order to describe the growth of the function p(n). The assumption is that the mean square displacement M(n) grows linearly as time passes when p(n) behaves asymptotical Brownian motion if the underlying dynamics is chaotic. The M(n) does not increase with n and is bounded if the underlying dynamics is non-chaotic.

Then growth rake K of the mean square displacement was then calculated as the result of linear regression of log M(n) versus log n. The result will therefore exhibit a clear difference between chaotic and a non-chaotic system. The chaotic characteristic of the system can be determined when K is close to 1. On the other hand, the system is determined to be non-chaotic is K is close to 0.

$$p(n) = \sum_{j=1}^{n} \Phi(j)\cos jc \tag{6}$$

$$M(n) = \lim_{N\to\infty} \frac{1}{N} \sum_{j=1}^{N} [p(j+n) - p(j)]^2 \tag{7}$$

$$K = \lim_{n\to\infty} \frac{\log M(n)}{\log n} \tag{8}$$

The translation variables p(n) is considered a part of the solution to the skew product system:

$$\theta(n+1) = \theta(n) + c, \tag{9}$$

$$p(n+1) = p(n) + \Phi(n)\cos\theta(n), \tag{10}$$

$$q(n+1) = q(n) + \Phi(n)\sin\theta(n), \tag{11}$$

(θ, p, q) is the coordinates on the Euclidean group. θ represents the rotation and

is the (p, q) represents position in the plane.

By simply looking at the plot of (p, q) trajectories, one can visually examine the chaotic characteristic of the underlying dynamics. If the behavior of p and q develops asymptotical motion along the line like Brownian motion, there is chaotic behavior in the system, the attractor is uniformly hyperbolic. At the meantime, the variance of the Brownian motion is nonzero for any observable $\Phi(n)$ and when $c > 0$. The underlying system should have a fast rate of decay of correlations in order to achieve $K = 1$.

For infinite number of data $\Phi(n)$ where $1 \leqslant n \leqslant N$, the formula can be modified as below.

$$M(n) = \frac{1}{N-n} \sum_{j=1}^{N-n} [p(j+n) - p(j)]^2 \tag{12}$$

In case of avoiding negative logarithms, use the equation below. And the slope K will not change.

$$K = \lim_{n \to \infty} \frac{\log M(n) + 1}{\log n} \tag{13}$$

For a small data size, certain choice of constant c might incur a resonance phenomenon. The choice of c resonates with the frequencies of the underlying dynamics, which makes the growth of the mean square displacement yield to n^2 and results in an unusual linear growth of p(n) with K=2. However, the cases of picking a bad choice of c are rare in practical experiments. The possibility of such bad choices is zero theoretically. In order to eliminate the resonance phenomenon, it is preferred to choose multiple values of c randomly, compute K for each choice of c, and take the median value of K. The method of taking median value of K instead of taking the

average of K is the result of eliminating weight of the irregular values of K.

2.5.2 Application of 0-1 Test on Theoretic Models

The 0-1 test is a straightforward and highly effective tool for uncovering deterministic chaos in nonlinear systems. The performance of the 0-1 test was evaluated in various experiments and literature in the past. The test has been applied to various well-understood nonlinear systems, and has been compared to other analytical methods. The effectiveness of the test was demonstrated.

Falconer et al (2007) constructed a bipolar motor system experimental setup and tested the data derived from it using 0-1 test in order to test the effectiveness of the test. The purpose of this experiment was to justify the performance of the 0-1 test in contaminated condition.

The bipolar motor was created by suspending a dipole magnet in a fixed, linearly polarized oscillating magnetic field. The motor was able to rotate around an axis freely. The angular position θ of the dipole magnet was recorded and a frequency of 25 times per second. The $\cos\theta$ was set as observable $\Phi(n)$. The final time series that the authors used for analysis duration contained 2700 data points.

The mean square displacement was calculated using the arbitrary choice c=1.95. The result shows dramatic difference between the bounded behavior which indicates the regular dynamics and the linear augment which indicates the chaotic behaviors. The asymptotic growth rate K of the mean square displacement was then determined using

c as a range between 0 and 2π. The values of the growth rate K as the function of c from 0 to 6.28 was acquired. The result shows demonstrated that except several unusual values, the majority of the c values yielded that K=0 for regular dynamics and K=1 for chaotic behaviors. The median of the K is used in order to avoid the weight of the exceptional values. The authors computed K for two experimental conditions with different frequencies of the magnetic field. The result of the computation was K=0.02 for 0.9Hz, periodic dynamics, and K=0.92 for 0.6Hz, chaos dynamics, which demonstrated that 0-1 test is able to distinguish chaotic behaviors. The authors also computed K using length of the time series N as a parameter. The result showed that with an increasing number N, the test obtained a better performance.

Gottwald and Melbourne (2003) also examined the 0-1 test in other cases. They applied the test method to investigate the forced van der Pol oscillator system. The chaotic behaviors were determined based on an unfixed parameter in the underlying equation that varied from 2.457 to 2.466, although the authors emphasized that the choices of the parameter would not affect the result. The value of c was equal to 1.7. The total time series contained 2,000,000 units of time. The result distinguished the onset of chaos dynamics when the parameter was equal or larger than 2.462. The result of the 0-1 test was compared to the result of the largest Lyapunov exponent using the same parameter in the same range. They both indicated same conclusion of regular dynamics when the parameter was smaller than 2.462 and both recorded the appearance of chaotic behaviors when the parameter was equal or larger than 2.462. The calculation result of K was K=0.01 for regular dynamics and K=0.8 for chaos dynamics. The

authors then carried out the 0-1 test again on the same system with less data quantity, containing 50,000 units of time. The result recorded the same onset point of chaos, except that the sensitivity of K was not as good as the test with larger data size.

The authors examined the 0-1 test on a high-dimensional system, namely damped Korteweg-de Vries (KdV) equations, in which the parameter β will result in regular solution when it is large, while lead to spatiotemporal chaos if it is adequately small. The 0-1 test was carried out for this equation. The result showed that when $\beta = 0$, $K = 0.939$, when $\beta = 0.1$, $K = 0.989$, and when $\beta = 4$, $K = 0.034$, which accorded with the assumptions of the equation. The authors then tested the method again on a discrete dynamical system with an ecological model which has a chaotic attractor. The 0-1 test succeeded to detect the chaotic behaviors ($K = 1.023$) with only 10,000 data points.

In another study, Gottwald and Melbourne (2005) examined if the 0-1 test could keep the performance in the presence of noise. The authors compared the 0-1 test to the maximal Lyapunov exponent in two experiments. In the first experiments, a logistic map was employed. The actual Lyapunov exponent was obtained directly from the map equation and was used as a benchmark. The approximate Lyapunov exponent was calculated from the phase space reconstruction. The result of the 0-1 test was compared to the maximal Lyapunov exponent calculated using the two methods mentioned above. The noise data with 1% noise level was added to the original data. The result showed that the addition of noise reduced the performance of the Lyapunov exponent with phase space reconstruction, but had little effect on the 0-1 test. The result of the 0-1 test was still consistent with the exact Lyapunov exponent. The authors then increased the noise

level to 10%, a more obvious deterioration in performance was observed for the maximal Lyapunov exponent. The performance of the 0-1 test, on the other hand, stayed the same.

The authors also compared the 0-1 test to the direct method for calculating the maximal Lyapunov exponent using the example of n-dimensional Lorenz system, also known as Lorenz 96 system. The same three indicators were calculated in order to test the capability of the two methods in terms of finding periodic windows in the system. In the noise-free environment, both methods found periodic windows correctly. However, when the noise level was increased to 10%, the maximal Lyapunov exponent began to exhibit much less distinguishable difference between chaotic and ordered dynamics. It also failed to recognize quasi-periodic windows from the chaos peaks. The 0-1 test was not influenced by the appearance of noise. The authors thus drew the conclusion that the 0-1 test was superior to the traditional chaos indicators in terms of noise toleration.

2.5.3 Application of 0-1 Test on Experimental Data

Litak et al (2009) investigated the chaotic vibration of a bouncing ball system which consisted of a ball that impacted on a kinematically forced plate while free falling in the Earth gravitational field and. This is an example of chaotic trajectories in the non-smooth mechanical systems. The authors stated that the 0-1 test had the advantage over the method of estimating the Lyapunov exponent given the absence of the equation of

the motion. It could be directly applied in the discontinuous system. However, the authors partially integrated the motions of the bouncing ball between the impacts. Thus the system could be directly investigated by both methods. The authors then examined the chaotic characteristics in the velocity of the kinematically forced plate after each impact, using the 0-1 test and the largest Lyapunov exponent respectively.

The maximal Lyapunov exponents were computed for two dimensionless driving frequencies q=20 and 22 and were plotted versus the impact numbers. The result indicated that the dynamics reached the definite value at the 250th impact, after which the chaotic or non-chaotic behaviors could be determined. When q= 20, there was a positive exponent suggesting a chaotic solution. While a negative exponent was obtained for q=22 indicating a regular solution.

The authors then applied the 0-test. The certain constant c was chosen as c = 1.7. The phase portraits of the plane of the translation variables p(n) and q(n) were already able to show that the distinction between Brownian trajectory (chaotic behaviors) when q=20 and the bounded trajectory (regular dynamics) when q = 22. The quantitative results of 0-1 test were K = 0.92 when q = 20 and K = 0.042 when q = 22, which confirmed the conclusion of the method of maximal Lyapunov exponent. The authors also plotted the all maximal Lyapunov exponents and K versus all parameter q from 15 to 25. The result indicated that these two methods agreed with each other constantly. And the experiments confirmed the practical performance of the 0-1 test in the experimental analysis. The phase portrait of translation variable (p, q) also illustrated the bounded circle trajectory for the regular dynamics and the unbounded trajectory for

the chaotic behaviors.

Yuasa and Saha (2007) repeated the study of the bouncing ball experiment in their study. They examined the time series of the vibration velocity when frequency q = 20 and q = 2. The calculation results of value K were near 1 in case of chaotic series and 0 in case of normal series, which supported the validation of the algorithm of the 0-1 test. In this study, a diffusive pattern of the translation variable, and the growth of the mean square displacement versus time were clearly observed for chaotic behaviors. The authors concluded that the 0-1 test was a reliable qualitative method for analyzing nonlinear dynamics.

Sun et al (2010) also compared the 0-1 test and the method of maximal Lyapunov exponent in their study. At first, the authors explore the different strategies of calculating the constant value c, using the example of the Hénon map. The experiments indicated that choosing the median value of K from 10 randomly chosen values of c could greatly mitigate the effect of the resonance phenomenon, although some periodic exceptional results still occurred. When calculating K from 100 random choices of values of c, the chance of resonance phenomenon almost disappeared. The authors then increased the total amount of value c to 1000. The result of the calculation did not show any further improvement. Thus the authors used 100 values of c in their calculation of K. According to the authors, the greater length of time series was able to help the 0-1 test improve its performance and reach its ideal value. The choice of parameter n was supposed to comply with the principle of $1 \leqslant n \leqslant N/10$. Nevertheless, the authors pointed out that the selection of n did not significantly affect the value of K in case of

chaotic behaviors. In the cases of regular dynamics, a smaller n could reduce the value of K and result in better distinction from chaotic behaviors.

The authors then applied both 0-test and the method of maximal Lyapunov exponent on the Hénon map, the integer-order simplified Lorenz system, and the fractional-order simplified Lorenz system. The result of the calculation showed great consistency between these two methods. The 0-1 test was considered to have lower computation cost regarding both effort and time. The 0-1 test was able to indicate a clear distinction of chaotic and non-chaotic behaviors. Furthermore, as a result of comparison the computation outcome for these two methods, the authors concluded that $K \leq 0.1$ referred to regular dynamics and $K > 0.1$ referred to chaotic behaviors. In this study, the phase portraits of the translation components for the three models were obtained. They all exhibited bounded shapes for the regular motion and asymptotic Brownian trajectory for the chaotic motion.

Dawes and Freeland (2008) investigated the performance of 0-1 test of distinguishing a strange nonchaotic attractor (SNA) in a quasi-periodic nonlinear system. The SNA cannot be detected by the method of the maximal Lyapunov exponent. It has a structure that is more complicated than normal dynamics. But it does not have a positive Lyapunov exponent for its separate rates are not as fast as exponential. The authors also offered a modification to the standard test procedure so that the test can better differentiate SNA. The authors used Fourier transformation and transferred the time series to smoothed time series in order to reduce the effect of noise. The authors then calculated the mean square displacement and its strength of increase K using the

Fourier transformed data. The calculation was repeated with different constant c that was distributed in the range from 0.1 to $\pi/2$. The median of K was selected in order to avoid the resonance effect. The refinement of the implement of the 0-1 test was accomplished by means of adding a noise term in the calculation of the mean square displacement. This modification was able to eliminate the frequent resonance effect generated from the quasi-periodic dynamics whose higher correlations would lead to erroneous numeric result of K = 1. The data that the authors used were generated from an original GOPY model. Compared with the standard test, value K in the modified version dropped significantly from 0.40683 to 0.0225608 for quasi-periodic structure but showed little difference for SNA. The result of the study demonstrated that the modified 0-1 test successfully recorded the onset of the SNA behavior of the quasi-periodic system.

Ascani et al (2008) also verified the capability of the 0-1 test to discover the chaos in quasi-periodic time series in their study. The authors applied the methods on time series generated from the Rössler model. The authors manipulated the parameter of the model and created two time series, one doubly-periodic and one chaotic. And then the authors added 10% white noise to the two noise-free time series respectively. Without the noise, the median of K values was 0.02 for the periodic data and 0.71 for the chaotic data. Given the presence of noise, the median of K values was 0.17 for the periodic data and 0.74 for the chaotic data. Therefore, the 0-1 test succeeded to distinguish the chaotic behaviors in the quasi-periodic time series even in a noisy condition. The authors also tested the performance of the 0-1 test on a surface electromyographic (sEMG) signals

witch captured the spinal waves derived by the muscle activities around the neck region in 30-second duration. The authors computed the maximal Lyapunov exponents for 10 segments of the time series, namely from 0 to 3 seconds, from 0 to 6 seconds, and so forth until the whole dataset. The false nearest neighbors (FNN) method was used to calculate the embedding dimension. After the phase space was reconstructed, the Lyapunov exponents for the group of time series were calculated. The positive maximal Lyapunov exponents were found in each segment, revealing the chaos in the sEMG recording. The authors then implemented the 0-1 test. They divided the data set into segments that consisted of 10 successive segments with identical time span, five successive segments with identical time span, and two successive segments with identical time span. The calculation was done for each of the time series segments and for the whole time series. The median value of K was selected with the 100 values of c ranging from $\pi/5$ to $4\pi/5$. The result showed that with the exception of only one of the 3-second segments, all values of K were greater than 0.75. All calculation indicated the existence of chaotic behaviors. The accuracy of the calculation increased along with the growth of the length of the data. The result of the two methods complied with each other. The authors tested the two methods again on a surrogate nondeterministic time series that were created based on the sEMG time series. The results of the two methods were still consistent with each other, which both mistakenly detected the false chaos, revealing the limitation of these nonlinear dynamics methods.

Budhraja et al (2012) verified the consistency between the 0-1 test and the maximal Lyapunov exponent. They tested the two methods on the Peter-de-Jong map

equations, which exhibited chaos or periodic behavior according to the variation of parameters. A total of 200,000 data units were generated from the model. The authors constructed 10 scenarios with different choice of parameters. They also compared the calculation results to the phase plot of the attractor. For the four scenarios in which the unbounded drifting phase plots suggested chaotic motion, the results of the 0-1 test and the maximal Lyapunov exponent both succeeded to detect the chaos. For three out of the four scenarios that have periodic form of attractors, both methods had results that were consistent with the phase plot, providing the signs of regular motion. For only one case, the trajectory of the attractor showed regular behavior. But a positive Lyapunov exponent was found. Besides, the value of K was 0.67571, according to the authors, indicating week chaos. Both of the mathematics methods had results that contradicted to the interpretation of the attractor. However, the authors did not provide any further explanation to the rare conflict. They concluded that the 0-1 test was as effective as the maximal Lyapunov exponent.

Because the 0-1 test can be carried out when the underlying equations of the data is unknown, it is favorable to adopt this method into various fields of practical or industrial applications where nonlinear processes are present. Litak et al (2009) studied the nonlinearity in a mechanical motion process of a machine. The authors employed the 0-1 test to predict the possible chaotic movement that could happen in a cutting sequence due to the friction, delay effect, structural factors, or contact loose effect between the tool and the work piece. The friction effect in the model resulted in non-smooth vector fields, and thus caused difficulty for computing Lyapunov exponents.

The calculation reached incorrect solutions for there were positive numbers for regular dynamics. Therefore the authors employed the 0-1 test in order to study the chaotic vibration generated in the cutting process, using the horizontal cutting depths for their time series data. The authors selected c=1.7 according to the reference of Gottwald and Melbourne. They calculated K versus four vertical cutting forces, namely 0.25, 0.5, 0.75, and 1. The result clearly distinguished the chaotic motion for the cutting force of 0.5 and 0.75 from the regular motion for the cutting force of 0.25 and 1. This result was supported by the phase portrait of (p, q) coordinates. The authors concluded that the 0-1 test was a reliable method for precise detection of the nonlinear chaos according to their study.

Gutnichenko et al (2014) studied the instability of high chromium cast iron (HCCI) in the cutting process with two polycrystalline cubic boron nitride (PCBN) tools. The instability was the result of the low-frequency vibration known as the “chatter” which was caused by the high hardness of the microstructural carbides constitutes. Under the influence of various factors, such as temperature and velocity dependent friction conditions, the “chatter” reflected the nonlinear interaction of tool and workpiece. Thus, the authors applied the nonlinear dynamics in their test as one of the indicators of the instability during machining, along with the specifics of tools wear mechanisms, the parameters of surface finish, and the morphology of the worn tools. In the experiment, two grades of PCBN tools were used on HCCI work pieces with two different chemical compositions and three different heat treatments. The acceleration amplitudes of the vibrations at different feeding rates were recorded. Afterward, the data was processed

by means of the 0-1 test. The result proved great stability for both of the two tools. The authors then verified the result by calculating the Lyapunov exponents. The result agreed with the previous conclusion, and confirmed the regular dynamics of the tools.

Chowdhury et al (2012) used the 0-1 test in order to investigate the nonlinearity in the time series of the potential fluctuation generated from a glow discharge plasma system. The plasma systems appear to have nonlinear dynamics and can have chaos or periodic behavior according to the change of parameters. The authors calculated the maximal Lyapunov exponent using Rosenstein's method. The result was 0.02 for quasi-periodic data and 0.2 for the chaotic data. The method clearly captured the existence of chaos. However, the value was close to zero for the quasi-periodic dynamics, indicating that it was a week indicator in this case. The 0-1 test was then carried out. The 100 values of constant c were chosen randomly varying from $\pi/5$ to $6\pi/5$. For the quasi-periodic dynamics, the numeric result of K was close to zero. The plot of mean square displacement showed there was no growth as time went on. For the chaotic behaviors, the median of K was proximately 0.9. The plot of mean square displacement depicted an obvious positive growing slope. The study proved the advantage of the 0-1 test over the maximal Lyapunov exponent in terms of accuracy regarding distinguishing quasi-periodic behavior.

Xu et al (2011) investigated the chaotic properties of a combustion process by means of the 0-1 test. According to the authors, there were nonlinear properties in the combustion process. Therefore, the combustion instability could be characterized by the existence of chaos. The authors applied 0-1 test to the nonlinear time series data

derived from the position series of the flame tip structures for different combination of fuel flow rates and air flow rates. For the results where the value K was equal to 0.8081, the authors concluded that the chaos happened. This conclusion was verified by the diffusive trajectory of the translation variable. For the results where K was below 0.8 and above 0.5, the author carried out further investigation using the recurrence plot method Poincaré section. The comparison leaded to the facts that when k was equal to 0.5046, the system was characterized as a periodic process. On the other hand, when values of k were equal to 0.6482 and 0.7646, the system was characterized as quasi-periodic processes. The authors implemented the 0-1 test twice by means of regression method function and correlation methods respectively. The difference was found in the numeric result for the two methods. However, they were both able to distinguish the condition in which the chaotic behaviors existed. The validity of the result was confirmed by the calculation of the maximal Lyapunov exponent.

The 0-1 test also serves as a tool for detecting chaos in time series in the financial research. Webel (2012) applied this method to examine the existence of chaotic structure in the financial time series data. The author estimated the daily stock returns from 30 companies in the German stock market. There were 1655 data units in the time series from each company. The authored used four kinds of wavelet filters in order to reduce the noise in the data, namely the least asymmetric, best localized, coiflet and the Haar filter. The multiple denoising methods were used in order to demonstrate that the filtering result was independent of the specific filter types. A total of 100 values of the constant c were randomly chosen in the range from $\pi/8$ to$7\pi/8$. The growth rate K was

calculated for each constant c and the median value was recorded as the final solution. According to the computation, the author successfully identified chaotic structure in the time series data from all 30 companies, drawing the conclusion that there was inherent deterministic chaos underlying the fluctuations of stock returns.

Kriz (2014) employed the 0-1 test to investigate if there was deterministic chaos in financial data using the example of the Finnish gross domestic product (GDP) data. Besides, the author verified the result of the 0-1 test with other methods, including the metric method such as the correlation dimension, the dynamical method such as computing the maximal Lyapunov exponent, and the topological method such as the recurrence plot. The author gathered quarterly data from year 1975 to 2012. There are two time series, namely seasonally adjusted data and data without adjustment. After the embedding dimension was determined by means of the "false nearest neighbors" method, the largest Lyapunov exponents was calculated using the Rosenstein algorithm. Positive maximal Lyapunov exponents were found in both time series, suggesting the existence of the chaotic behavior. The 0-1 test was then implemented. The value of the correlation coefficient was calculated as 0.95 for both time series. The correlation dimension was also computed using Grassberger and Procaccia algorithm. The values of Hurst exponent for the two time series were both close to 1, indicating the existence of long-range dependence. The recurrence plots presented irregular diagonal structures, which also confirmed that there was chaotic structure in the time series. The author concluded that all the methods mentioned above corresponded with each other and reached same result of chaotic structure for both time series.

CHAPTER 3: OBJECTIVES

3.1 Problem statement

The objective of this study is to examine the mental workload under different task difficulty levels through the investigation of brain activity by means of nonlinear dynamics of EEG recordings in simulated unmanned ground vehicle visual detection task scenarios. It is hypothesized that EEG associated with mental workload exhibits chaotic behavior. Furthermore, increased mental workload is associated with higher level of chaos in corresponding EEG pattern. The main research tasks include:

1), Does the level of chaotic behaviors in EEG data varies according to the changes of task difficulty?

2), How does the change in brain activity reflect the effect of mental workload?

The first task aims to find the change of nonlinearity levels in EEG recordings for different task difficulty. If significant changes of EEG nonlinearity occur, it is indicated that varying task difficulty is able to cause the change in performers' brain activity, and that brain activity is an indicator of mental work. As a result, the next task will occur regarding what parts of brain are affected by different level of mental workload, and affected in what way. It would be necessary to investigate the pattern of the changes in brain activity in order to understand how they are influenced by variation of mental workload.

3.2 Research Hypothesis

There are two hypotheses in this research. The first one is that the EEG associated with mental workload will exhibit chaotic behavior. Secondly, the varied mental workload associates with different level of chaos in corresponding EEG pattern.

CHAPTER 4: RESEARCH METHODOLOGY

4.1 Participants

One-hundred and fifty graduate and undergraduate student volunteers, including 85 males and 65 females, whose average age was 19.57 with standard deviation 3.46, participated in the experiment. Informed consent was obtained from the participants. All participants were screened for normal or corrected-to-normal vision and had zero previous experience with the simulator prior to participation. Subjects also had no ingestion of alcohol, and/or sedative medications at least 24 hours prior to participation, as well as no ingestion of caffeine, and/or nicotine at least 2 hours prior to participation, in order to ensure the validity of physiological measures.

4.2 Apparatus

The tasks were performed in a simulated operator control unit (OCU) for an unmanned ground vehicle (UGV) using the Mixed Initiative eXperimental (MIX) testbed, designed by Reinerman-Jones et al (2010). The UGV navigated through an environment which appeared to be a generic Middle Eastern town seized by enemy threats. The UGV drove autonomously along a prefixed route. Participants were expected to identify the occurrence of enemy targets on the way. A desktop computer (3.2GHz, Intel Core i7 processor) with a 22" (16:10 aspect ratio) monitor was used as display device for this simulation. The participants' responses to the task were collected by means of clicking the left mouse button.

4.3 Tasks

The tasks designed by Reinerman-Jones et al (2010) included two parts and were performed by participants independently, namely threat detection (TD) task and the change detection (CD). These two tasks were also performed simultaneously, forming a dual-task scenario. These tasks resembled the real military intelligence, surveillance and reconnaissance missions with a simulated unmanned vehicle operation. The threat detection task was chosen base on signal detection theory (SDT). According to SDT, decisions are made in the presence of uncertainty due to the presence of either internal that comes from perceptual processing and/or neural activity and/or external noise that comes from environmental sources. Thus, it is crucial to determine the decision-making criteria in order to mitigate unwanted results or workload in a high-risk environment. The change detection task was chosen based on the theories of change blindness (CB), which refers to the situation in which the observer fails to notice changes in a visual scene. Change detection requires the ability of attention allocation which closely related to workload level. As a result, workload exerts a strong influence on the performance of change detection tasks.

Figure 1 The Tasks in The Unmanned Ground Vehicle System (Reinerman-Jones et al, 2010).

4.3.1 Threat Detection Task

As shown in Figure 1, in the threat detection task, participants were asked to monitor a video feed projecting the forward view of the UGV that drove along a prefixed route and report any potential threats present. Among the four categories of people that were presented, namely friendly soldiers, friendly civilians, enemy soldiers, and insurgents, the last two were considered as threats and were reported by a left-clicking of the computer mouse on the “threat detect” button located on the top right of the OCU followed by another left-clicking on the threat in the UGV video feed.

4.3.2 Change Detection Task

In the change detection task, participants were asked to monitor an aerial map located at the bottom of the OCU that displayed the location of various icons. There were an average of 24 icons presented randomly across the defined area. Three types of changes of the icons were exhibited, namely appear, disappear and movement. Three change detection buttons representing each type of change were positioned above the aerial map. The identified icon changes were reported by a left-clicking of the computer mouse on the appropriate change detection button.

4.3.3 Task Procedure

Participants were trained and were provided with a practice session. The full experiments consisted of four scenarios. There were two single task scenarios, in which participants performed the change detection task only or threat detection task only. There were also two dual task scenarios, in which participants performed the change detection task at a varied event rate, while event rate of the threat detection task kept at a constant level, or vice versa, performed the TD task at a varied event rate, while the CD task kept at a constant level. Three levels of event rate were utilized within each scenario, as presented in Table 1, representing low, medium, and high task levels.

For the change detection single task (Scenario 1): the event rate 6, 12, and 24 per minute was used. For the change detection dual task (Scenario 2): the event rate was 6,

12, and 24 per minute for the change detection task, as well as 30 per minute for threat detection task. For the threat detection single task (Scenario 3): the event rate was used 15, 30, and 60 per minute. On the other hand, for the threat detection dual task (Scenario 4), the event rate was 15, 30, and 60 per minute for change detection task, as well as 12 per minute for the threat detection task. The order of the task scenarios that represented different workload levels was counterbalanced and randomized for each participant.

After performing the tasks, the subjective workload measure NASA Task Load Index (Hart & Staveland, 1988), also known as NASA-TLX, scores of the participants were recorded. NASA-TLX assesses subjective mental workload on six dimensions, namely mental demand, physical demand, temporal demand, performance, effort, and frustration level. It employs a weighting procedure, in which the dimensions will be selected if they are more relevant to workload, so that the multiple subscales used in this technique can eventually combine together and provide a unidimensional estimation of mental workload. The task load manipulation of low, medium, and high level resulted in corresponding level of subjective workload measure.

The mean and standard deviation of the NASA-TLX data recorded by Mathews et al (2014) are shown in Table 2. The two dual tasks both have higher subjective measures than the single tasks. For the two single tasks, change detection task has higher NASA-TLX than threat detection task. For both change detection tasks and threat detection tasks, the increased task difficulty level has significant effect on the subjective mental workload measurements, when compare the dual task with the single task. However, there is no significant effect between the two single tasks (Mathews et

al, 2014).

Table 1 Task event rate per minute under different task scenarios

	Change Detection Single Task (S1)	Change Detection Dual Task (S2)	Threat Detection Single Task (S3)	Threat Detection Dual Task (S4)
Change Detection Event Rate	6	6		12
	12	12		
	24	24		
Threat Detection Event Rate		30	15	15
			30	30
			60	60

Table 2 NASA task load index under different task scenarios

NASA-TLX	Mean	Standard Deviation
Change Detection Single Task (S1)	47.67	14.20
Change Detection Dual Task (S2)	57.68	14.51
Threat Detection Single Task (S3)	31.58	16.53
Threat Detection Dual Task (S4)	56.31	19.92

4.4 EEG Data Acquisition

The EEG data was collected for each of the one-hundred and fifty participants from an Advanced Brain Monitoring X10 system while they performed the four single and dual task scenarios throughout the five-minute duration with a sampling rate at 256 Hz. The EEG was recorded at nine channels located at frontal, central, and parietal locations, namely F3, Fz, F4, C3, Cz, C4, P3, Pz, and P4. The baseline EEG was recorded while the participants were resting and used as reference. In Figure 2, a sample of the EEG time series data for a central parietal channel from one subject is shown.

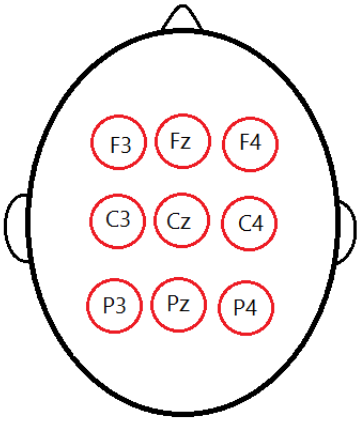

Figure 2 The distribution map of the EEG channels.

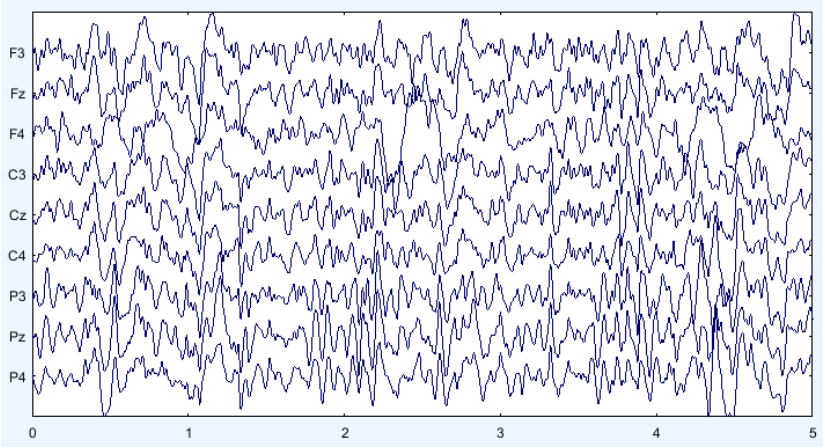

Figure 3 Sample EEG data from subject one central parietal channel, scenario 1 condition.

4.5 Methodology

4.5.1 Data Processing

Due to the large amount of EEG data set and the enormous volume of the data. I developed the first part of the program via software Python as a file loader. The data of each EEG channel can be separated from one data file, which contains the data of all nine EEG channels for one subject, and transpose from multiple rows into one column. Each file can be automatically loaded from the file folder into Python software and be

ready for further computation.

4.5.2 Lyapunov Exponent And Fractal Dimension

The two parameters that are used to calculate the largest Lyapunov exponent and the correlation dimension, namely time delay and embedding dimension, are calculated for each task scenario, via software Matlab.

The embedding dimension m was calculated using false nearest neighbors (FNN) algorithm. According to the FNN algorithm, a chaotic time series is a projection of the dynamics from a higher-dimensional phase space to a lower-dimensional phase space. Thus, two nearest points in the lower dimensional phase space are considered false nearest neighbors due to they are not close to each other in the higher dimensional phase space, which is the reason why the time series exhibits chaotic dynamics. Phase space reconstruction is a process of embedding the time series into higher dimensional phase space, until all false nearest neighbors are separated. The FNN algorithm finds the true neighbors that remain close when the data are embedded into a higher dimensional space. When FNN is detected, the minimal embedding dimension is also recognized, which is the situation when as the embedding dimension increases, the fraction of the FNN changes less than 5%.

The time delay τ was calculated by means of estimating the autocorrelation in the time series. The autocorrelation function for a series of continuous variables is defined as

$$C(\tau) = \lim_{T\to\infty} \int_{-\frac{T}{2}}^{\frac{T}{2}} x(t)x(t+\tau)dt \quad (14)$$

τ is the time lag, representing the level of correlation between two points in time (t and t+ τ). τ is determined when it is large enough so that x(t) and x(t+ τ) have less difference, where $C(\tau)$ approaches zero.

After the phase space was reconstructed for the EEG time series data, the largest Lyapunov exponent was computed using Rosenstein method (1993). The correlation dimension was estimated using the method developed by Grassberger and Procaccia (1983), using software Python.

4.5.3 0-1 Test

The 0-1 test for chaos was applied to the EEG time series of each of the nine EEG channels of each of the one-hundred and fifty participants for all four task scenarios and for the resting baseline, using the algorithm that I developed on software Python. The parameter of c was chosen from a randomly generated string of values between 1/5 π and 4/5 π. So that the selection of median Kc was able to mitigate the resonance effect. A K value was obtained for each EEG channel for every participant and for every scenario. The K value close to 1 indicates the existence of chaos and the K value close to 0 indicates a regular dynamics.

4.5.4 Statistical Analysis

The relationship between the task demand of each scenario and changes in brain activity was examined via the one-way analysis of variance (ANOVA) using software Minitab, among the same EEG channel's largest Lyapunov exponent, correlation dimension, and K value for different task scenarios and the resting baseline.

The effect of task difficulty was further investigated via ANOVA using software Minitab among the nine EEG channels for different level of tasks, in order to examine at which areas of the brain the shifting mental workload levels has an effect on brain activity.

CHAPTER 5: RESULTS

5.1 Lyapunov Exponent

The EEG data was bandpass filtered using FIR filter from 4Hz to 30Hz, in the range from Theta to Beta brain wave, in order to eliminate the effect of eye blink. The embedding dimensions for scenario 1, scenario 2, scenario 3, and scenario 4 are shown in Table 3. The time delay for scenario 1, scenario 2, scenario 3, and scenario 4 are shown in Table 4. The same parameters were also employed in the calculation of correlation dimension.

Table 3 The embedding dimension for each task scenario

Task Scenario	Embedding Dimension
Change Detection Single Task (S1)	8
Change Detection Dual Task (S2)	8
Threat Detection Single Task (S3)	7
Threat Detection Single Task (S4)	10

Table 4 The time delay for each task scenario

Task Scenario	Time Delay
Change Detection Single Task (S1)	4
Change Detection Dual Task (S2)	4
Threat Detection Single Task (S3)	5
Threat Detection Single Task (S4)	3

The positive largest Lyapunov exponents are observed in all EEG time series, which can be considered as the evidence that supported the existence of the chaotic dynamics in EEG time series.

5.1.1 Task Levels

One-way ANOVA was performed on the results of Lyapunov exponent in order to examine the effect of varying task levels. Significant difference in Lyapunov exponent was found between medium and high task levels for change detection single task (p-value = 0.31). Marginally significant effect was found between low and medium task levels also for change detection single task (p-value = 0.110). However, there was no significant difference for other task scenarios when the task difficulty levels change. The grouping information of mean values was determined by Fisher's least significant difference test. When the task difficulty level changed from low level to medium level, the marginally significant change in Lyapunov exponent was found in change detection single task at EEG channel C3, located at left central sulcus (p-value = 0.173). When

the task level shift from medium to high level, marginally significant change in Lyapunov exponent was found also found in change detection single task at channel C3 (p-value = 0.054) and P3 (p-value = 0.105), located at left central sulcus and right parietal lobe.

Table 5 Comparison of the largest Lyapunov exponent for different task levels

Scenario	Task Level	Mean	Grouping	Standard Deviation
Change Detection Single Task (S1)	Low	0.014844	A	0.002228
	Medium	0.014983	A	0.002180
	High	0.014793	B	0.002283
Change Detection Dual Task (S2)	Low	0.014881	A	0.002267
	Medium	0.014832	A	0.002218
	High	0.014756	A	0.002237
Threat Detection Single Task (S3)	Low	0.013989	A	0.001780
	Medium	0.013972	A	0.001907
	High	0.013895	A	0.001877
Threat Detection Dual Task (S4)	Low	0.015151	A	0.002479
	Medium	0.015150	A	0.002729
	High	0.015116	A	0.002545

Table 6 ANOVA table of the largest Lyapunov exponent for change detection single task (S1) between low and medium level.

Source of Variation	Degrees of Freedom	Sum of Squares	Mean Squares	F	p Value
Scenario	1	0.000012	0.000012	2.55	0.110
Error	2545	0.012365	0.000005		
Total	2546	0.012378			

Table 7 ANOVA table of the largest Lyapunov exponent for change detection single task (S1) between medium and high level.

Source of Variation	Degrees of Freedom	Sum of Squares	Mean Squares	F	p Value
Scenario	1	0.000023	0.000023	4.65	0.031
Error	2554	0.012727	0.000005		
Total	2555	0.012750			

Table 8 ANOVA table of the largest Lyapunov exponent for change detection single task (S1) between low and medium level at channel C3.

Source of Variation	Degrees of Freedom	Sum of Squares	Mean Squares	F	p Value
Scenario	1	0.000008	0.000008	1.86	0.173
Error	281	0.001187	0.000004		
Total	282	0.001194			

Table 9 ANOVA table of the largest Lyapunov exponent for change detection single task (S1) between medium and high level at channel C3.

Source of Variation	Degrees of Freedom	Sum of Squares	Mean Squares	F	p Value
Scenario	1	0.000016	0.000016	3.75	0.054
Error	282	0.001208	0.000004		
Total	283	0.001224			

Table 10 ANOVA table of the largest Lyapunov exponent for change detection single task (S1) between medium and high level at channel P3.

Source of Variation	Degrees of Freedom	Sum of Squares	Mean Squares	F	p Value
Scenario	1	0.000011	0.000011	2.65	0.105
Error	282	0.001137	0.000004		
Total	283	0.00114			

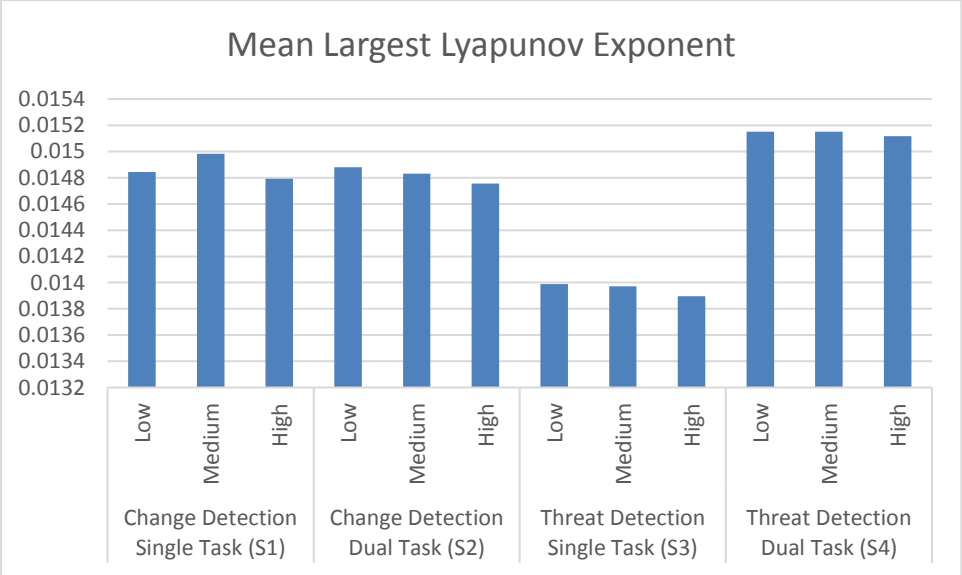

Figure 4 Comparison of the largest Lyapunov exponent for different task levels.

5.1.2 Change Detection Tasks Single And Dual Task Scenarios

One-way ANOVA was then performed on the single and dual change detection tasks for each of the three task levels in order to examine the effect of the difference between single task and dual task on the change in the nonlinearity of EEG. There was no significant difference found at any task level. There was only marginally significant difference in Lyapunov exponent found at the medium level (p-value = 0.081). After examining the EEG channels, the marginally significant effect between single change detection task and dual change detection task was found at C3, left central sulcus, at the medium task level.

Table 11 The mean largest Lyapunov exponent for change detection tasks at different task level

Task Level	Scenario	Mean	Grouping	Standard Deviation
Low	Change Detection Single Task (S1)	0.014844	A	0.002228
	Change Detection Dual Task (S2)	0.014881	A	0.002267
Medium	Change Detection Single Task (S1)	0.014983	A	0.002180
	Change Detection Dual Task (S2)	0.014832	A	0.002218
High	Change Detection Single Task (S1)	0.014793	A	0.002283
	Change Detection Dual Task (S2)	0.014756	A	0.002237

Table 12 ANOVA table of the largest Lyapunov exponent for change detection single and dual tasks at medium task level.

Source of Variation	Degrees of Freedom	Sum of Squares	Mean Squares	F	p Value
Scenario	1	0.000015	0.000015	3.05	0.081
Error	2563	0.012399	0.000005		
Total	2564	0.012413			

Table 13 ANOVA table of the largest Lyapunov exponent for change detection tasks at medium task level at channel C3.

Source of Variation	Degrees of Freedom	Sum of Squares	Mean Squares	F	p Value
Scenario	1	0.000014	0.000014	2.98	0.085
Error	283	0.001292	0.000005		
Total	284	0.001306			

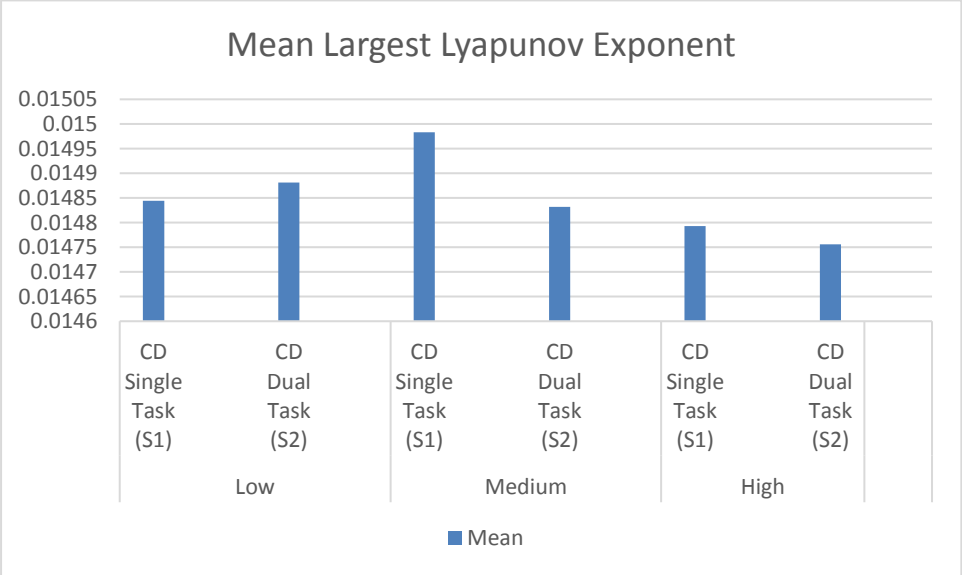

Figure 5 Comparison of the largest Lyapunov exponent for change detection (CD) tasks.

5.1.3 Threat Detection Task Single And Dual Task Scenarios

One-way ANOVA was also performed on the single and dual threat detection tasks in order to investigate the effect of switching from single task to dual task on the

change in the nonlinearity of EEG. For all of the three task levels, the significant effect was found between the single task scenario and the dual task scenario (p-value < 0.001). The dual task scenarios were significantly different from the single task scenarios at all EEG channels (p-value < 0.05).

Table 14 The mean largest Lyapunov exponent for threat detection tasks at different task level

Task Level	Scenario	Mean	Grouping	Standard Deviation
Low	Threat Detection Single Task (S3)	0.013989	B	0.001780
	Threat Detection Dual Task (S4)	0.015151	A	0.002479
Medium	Threat Detection Dual Task (S3)	0.013972	B	0.001907
	Threat Detection Dual Task (S4)	0.015150	A	0.002729
High	Threat Detection Single Task (S3)	0.013895	B	0.001877
	Threat Detection Dual Task (S4)	0.015116	A	0.002545

Table 15 ANOVA table of the largest Lyapunov exponent for threat detection single and dual tasks at low task level.

Source of Variation	Degrees of Freedom	Sum of Squares	Mean Squares	F	p Value
Scenario	1	0.000857	0.000857	183.95	0.000
Error	2536	0.011812	0.000005		
Total	2537	0.012669			

Table 16 ANOVA table of the largest Lyapunov exponent for threat detection single and dual tasks at medium task level.

Source of Variation	Degrees of Freedom	Sum of Squares	Mean Squares	F	p Value
Scenario	1	0.000891	0.000891	160.87	0.000
Error	2563	0.014192	0.000006		
Total	2564	0.015083			

Table 17 ANOVA table of the largest Lyapunov exponent for threat detection single and dual tasks at high task level.

Source of Variation	Degrees of Freedom	Sum of Squares	Mean Squares	F	p Value
Scenario	1	0.000953	0.000953	190.54	0.000
Error	2554	0.012775	0.000005		
Total	2555	0.013728			

Table 18 ANOVA table of the largest Lyapunov exponent for threat detection tasks at low task level at channel C3.

Source of Variation	Degrees of Freedom	Sum of Squares	Mean Squares	F	p Value
Scenario	1	0.000084	0.000084	18.52	0.000
Error	280	0.001274	0.000005		
Total	281	0.001358			

Table 19 ANOVA table of the largest Lyapunov exponent for threat detection tasks at low task level at channel C4.

Source of Variation	Degrees of Freedom	Sum of Squares	Mean Squares	F	p Value
Scenario	1	0.000089	0.000089	20.74	0.000
Error	280	0.001196	0.000004		
Total	281	0.001284			

Table 20 ANOVA table of the largest Lyapunov exponent for threat detection tasks at low task level at channel Cz.

Source of Variation	Degrees of Freedom	Sum of Squares	Mean Squares	F	p Value
Scenario	1	0.000074	0.000074	14.98	0.000
Error	280	0.001384	0.000005		
Total	281	0.001458			

Table 21 ANOVA table of the largest Lyapunov exponent for threat detection tasks at low task level at channel F3.

Source of Variation	Degrees of Freedom	Sum of Squares	Mean Squares	F	p Value
Scenario	1	0.000097	0.000097	20.22	0.000
Error	280	0.001346	0.000005		
Total	281	0.001443			

Table 22 ANOVA table of the largest Lyapunov exponent for threat detection tasks at low task level at channel F4.

Source of Variation	Degrees of Freedom	Sum of Squares	Mean Squares	F	p Value
Scenario	1	0.000066	0.000066	16.20	0.000
Error	280	0.001149	0.000004		
Total	281	0.001215			

Table 23 ANOVA table of the largest Lyapunov exponent for threat detection tasks at low task level at channel Fz.

Source of Variation	Degrees of Freedom	Sum of Squares	Mean Squares	F	p Value
Scenario	1	0.000026	0.000026	4.38	0.037
Error	280	0.001634	0.000006		
Total	281	0.001660			

Table 24 ANOVA table of the largest Lyapunov exponent for threat detection tasks at low task level at channel P3.

Source of Variation	Degrees of Freedom	Sum of Squares	Mean Squares	F	p Value
Scenario	1	0.000141	0.000141	34.04	0.000
Error	280	0.001158	0.000004		
Total	281	0.001299			

Table 25 ANOVA table of the largest Lyapunov exponent for threat detection tasks at low task level at channel P4.

Source of Variation	Degrees of Freedom	Sum of Squares	Mean Squares	F	p Value
Scenario	1	0.000162	0.000162	41.22	0.000
Error	280	0.001099	0.000004		
Total	281	0.001261			

Table 26 ANOVA table of the largest Lyapunov exponent for threat detection tasks at low task level at channel Pz.

Source of Variation	Degrees of Freedom	Sum of Squares	Mean Squares	F	p Value
Scenario	1	0.000168	0.000168	40.58	0.000
Error	280	0.001160	0.000004		
Total	281	0.001328			

Table 27 ANOVA table of the largest Lyapunov exponent for threat detection tasks at medium task level at channel C3.

Source of Variation	Degrees of Freedom	Sum of Squares	Mean Squares	F	p Value
Scenario	1	0.000127	0.000127	26.03	0.000
Error	283	0.001379	0.000005		
Total	284	0.001506			

Table 28 ANOVA table of the largest Lyapunov exponent for threat detection tasks at medium task level at channel C4.

Source of Variation	Degrees of Freedom	Sum of Squares	Mean Squares	F	p Value
Scenario	1	0.000084	0.000084	17.26	0.000
Error	283	0.001380	0.000005		
Total	284	0.001464			

Table 29 ANOVA table of the largest Lyapunov exponent for threat detection tasks at medium task level at channel Cz.

Source of Variation	Degrees of Freedom	Sum of Squares	Mean Squares	F	p Value
Scenario	1	0.000053	0.000053	10.84	0.001
Error	283	0.001381	0.000005		
Total	284	0.001434			

Table 30 ANOVA table of the largest Lyapunov exponent for threat detection tasks at medium task level at channel F3.

Source of Variation	Degrees of Freedom	Sum of Squares	Mean Squares	F	p Value
Scenario	1	0.000126	0.000126	19.06	0.000
Error	283	0.001876	0.000007		
Total	284	0.002002			

Table 31 ANOVA table of the largest Lyapunov exponent for threat detection tasks at medium task level at channel F4.

Source of Variation	Degrees of Freedom	Sum of Squares	Mean Squares	F	p Value
Scenario	1	0.000137	0.000137	19.21	0.000
Error	283	0.002023	0.000007		
Total	284	0.002161			

Table 32 ANOVA table of the largest Lyapunov exponent for threat detection tasks at medium task level at channel Fz.

Source of Variation	Degrees of Freedom	Sum of Squares	Mean Squares	F	p Value
Scenario	1	0.000035	0.000035	6.63	0.011
Error	283	0.001512	0.000005		
Total	284	0.001547			

Table 33 ANOVA table of the largest Lyapunov exponent for threat detection tasks at medium task level at channel P3.

Source of Variation	Degrees of Freedom	Sum of Squares	Mean Squares	F	p Value
Scenario	1	0.000119	0.000119	26.71	0.000
Error	283	0.001265	0.000004		
Total	284	0.001384			

Table 34 ANOVA table of the largest Lyapunov exponent for threat detection tasks at medium task level at channel P4.

Source of Variation	Degrees of Freedom	Sum of Squares	Mean Squares	F	p Value
Scenario	1	0.000100	0.000100	17.87	0.000
Error	283	0.001579	0.000006		
Total	284	0.001678			

Table 35 ANOVA table of the largest Lyapunov exponent for threat detection tasks at medium task level at channel Pz.

Source of Variation	Degrees of Freedom	Sum of Squares	Mean Squares	F	p Value
Scenario	1	0.000144	0.000144	32.72	0.000
Error	283	0.001246	0.000004		
Total	284	0.001390			

Table 36 ANOVA table of the largest Lyapunov exponent for threat detection tasks at high task level at channel C3.

Source of Variation	Degrees of Freedom	Sum of Squares	Mean Squares	F	p Value
Scenario	1	0.000150	0.000150	35.74	0.000
Error	282	0.001184	0.000004		
Total	283	0.001334			

Table 37 ANOVA table of the largest Lyapunov exponent for threat detection tasks at high task level at channel C4.

Source of Variation	Degrees of Freedom	Sum of Squares	Mean Squares	F	p Value
Scenario	1	0.000154	0.000154	35.61	0.000
Error	282	0.001218	0.000004		
Total	283	0.001372			

Table 38 ANOVA table of the largest Lyapunov exponent for threat detection tasks at high task level at channel Cz.

Source of Variation	Degrees of Freedom	Sum of Squares	Mean Squares	F	p Value
Scenario	1	0.000062	0.000062	11.31	0.001
Error	282	0.001545	0.000005		
Total	283	0.001607			

Table 39 ANOVA table of the largest Lyapunov exponent for threat detection tasks at high task level at channel F3.

Source of Variation	Degrees of Freedom	Sum of Squares	Mean Squares	F	p Value
Scenario	1	0.000133	0.000133	23.07	0.000
Error	282	0.001620	0.000006		
Total	283	0.001752			

Table 40 ANOVA table of the largest Lyapunov exponent for threat detection tasks at high task level at channel F4.

Source of Variation	Degrees of Freedom	Sum of Squares	Mean Squares	F	p Value
Scenario	1	0.000123	0.000123	22.60	0.000
Error	282	0.001532	0.000005		
Total	283	0.001655			

Table 41 ANOVA table of the largest Lyapunov exponent for threat detection tasks at high task level at channel Fz.

Source of Variation	Degrees of Freedom	Sum of Squares	Mean Squares	F	p Value
Scenario	1	0.000045	0.000045	7.34	0.007
Error	282	0.001718	0.000006		
Total	283	0.001763			

Table 42 ANOVA table of the largest Lyapunov exponent for threat detection tasks at high task level at channel P3.

Source of Variation	Degrees of Freedom	Sum of Squares	Mean Squares	F	p Value
Scenario	1	0.000116	0.000116	28.15	0.000
Error	282	0.001164	0.000004		
Total	283	0.001280			

Table 43 ANOVA table of the largest Lyapunov exponent for threat detection tasks at high task level at channel P4.

Source of Variation	Degrees of Freedom	Sum of Squares	Mean Squares	F	p Value
Scenario	1	0.000108	0.000108	26.16	0.000
Error	282	0.001160	0.000004		
Total	283	0.001268			

Table 44 ANOVA table of the largest Lyapunov exponent for threat detection tasks at high task level at channel Pz.

Source of Variation	Degrees of Freedom	Sum of Squares	Mean Squares	F	p Value
Scenario	1	0.000093	0.000093	23.72	0.000
Error	282	0.001109	0.000004		
Total	283	0.001202			

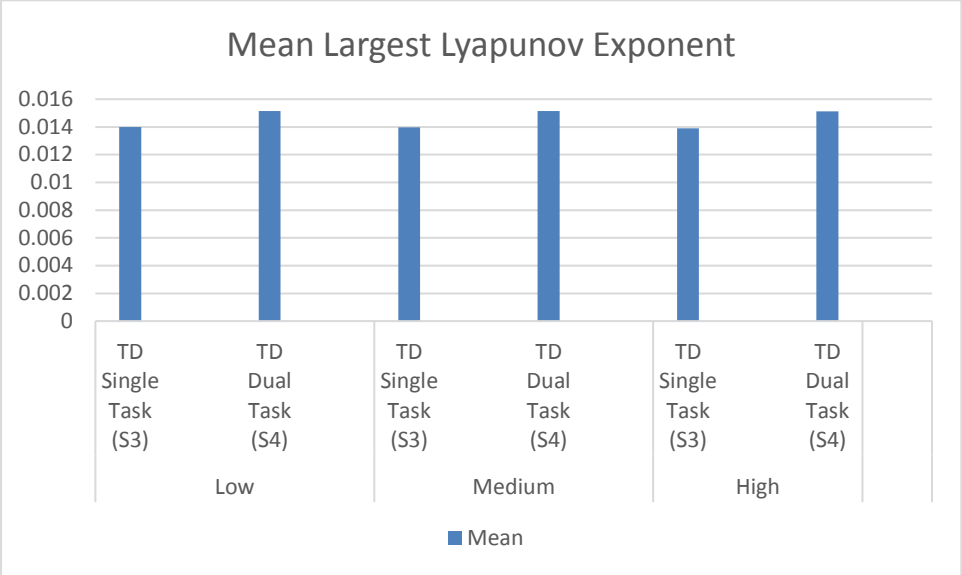

Figure 6 Comparison of the largest Lyapunov exponent for threat detection (TD) tasks.

5.2 Fractal Dimension

5.2.1 Task Levels

As shown in Figure 7 to Figure 10, the phase portraits of the attractors demonstrate that the strange attractors were found in EEG time series data, indicating the existence of chaos phenomena in these EEG time series. One-way ANOVA was performed on the results of correlation dimensions in order to determine the significant effect of the task level differences. The results have found that the correlation dimensions differed significantly for change detection dual task between low and medium task level (p-value = 0.024) and for threat detection single task between medium and high task level (p-value < 0.001). There was also marginally significant change in correlation dimension for change detection single task between low and medium task level (p-value = 0.078).

Table 45 Comparison of correlation dimension for different task levels

Scenario	Task Level	Mean	Grouping	Standard Deviation
Change Detection Single Task (S1)	Low	2.0419	A	1.1245
	Medium	1.9641	A	1.1033
	High	1.9527	A	1.1032
Change Detection Dual Task (S2)	Low	2.0006	A	1.1100
	Medium	1.9019	B	1.1063
	High	1.9523	B	1.1111
Threat Detection Single Task (S3)	Low	2.3188	A	0.9215
	Medium	2.3253	A	0.8942
	High	2.2019	B	0.8878
Threat Detection Dual Task (S4)	Low	1.7419	A	1.2123
	Medium	1.7088	A	1.2073
	High	1.6564	A	1.2073

Table 46 ANOVA table of correlation dimension for change detection single task (S1) between low and medium level.

Source of Variation	Degrees of Freedom	Sum of Squares	Mean Squares	F	p Value
Scenario	1	3.86	3.858	3.11	0.078
Error	2545	3157.88	1.241		
Total	2546	3161.74			

Table 47 ANOVA table of correlation dimension for change detection dual task (S2) between low and medium level.

Source of Variation	Degrees of Freedom	Sum of Squares	Mean Squares	F	p Value
Scenario	1	6.27	6.272	5.11	0.024
Error	2572	3158.60	1.228		
Total	2573	3164.87			

Table 48 ANOVA table of correlation dimension for threat detection single task (S3) between medium and high level.

Source of Variation	Degrees of Freedom	Sum of Squares	Mean Squares	F	p Value
Scenario	1	9.77	9.7701	12.31	0.000
Error	2563	2034.83	0.7939		
Total	2564	2044.60			

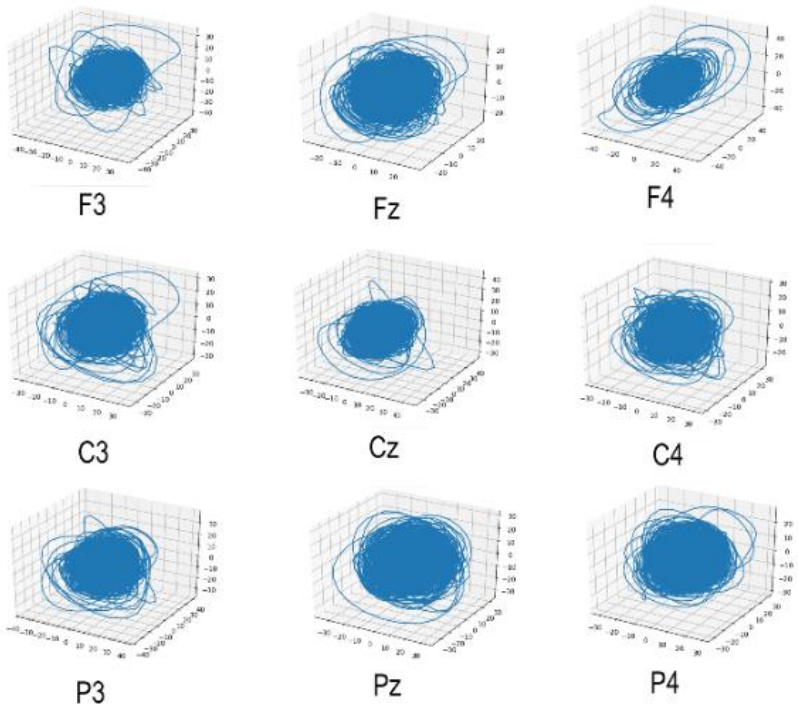

Figure 7 Phase portraits of attractors of EEG time series for change detection single task (S1).

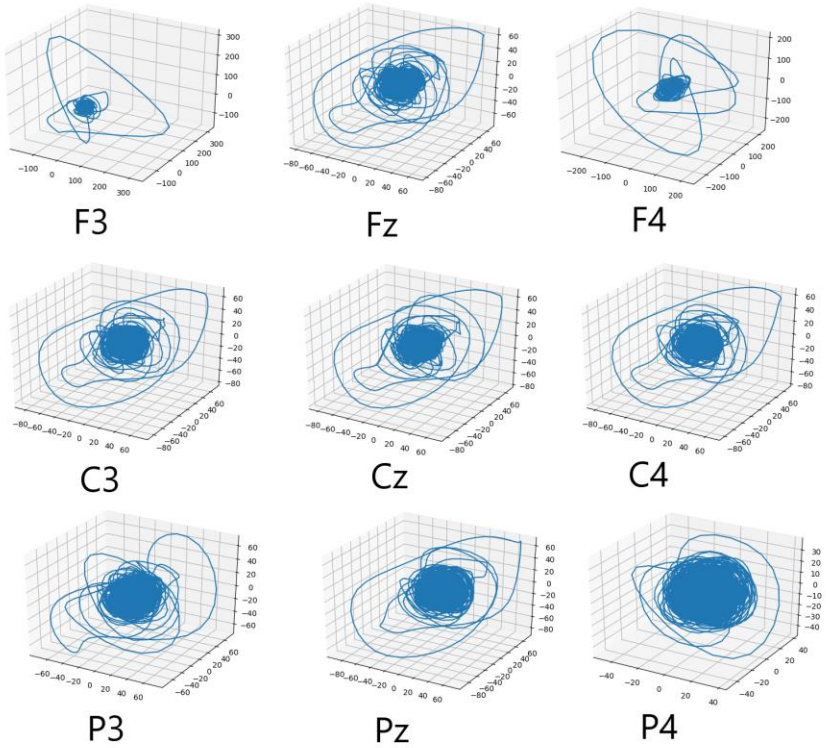

Figure 8 Phase portraits of attractors of EEG time series for change detection dual task (S2).

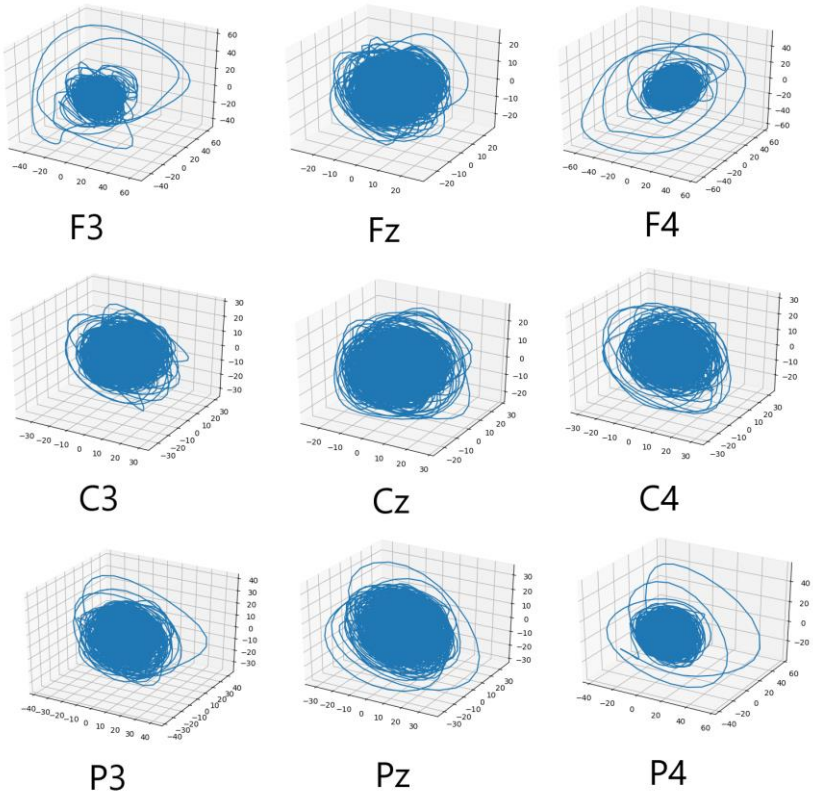

Figure 9 Phase portraits of attractors of EEG time series for threat detection single task (S3).

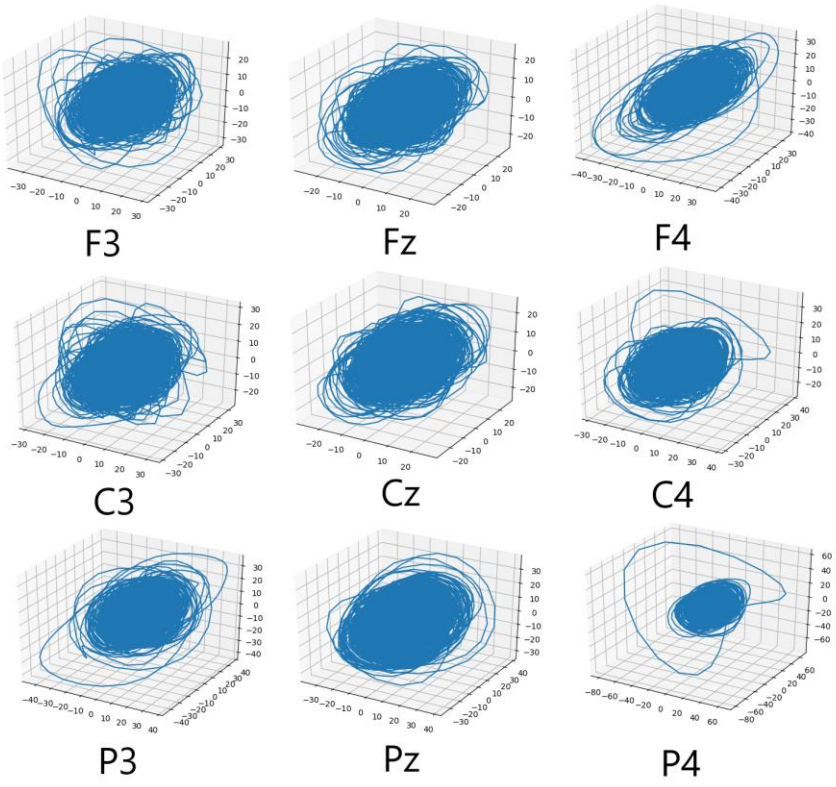

Figure 10 Phase portraits of attractors of EEG time series for threat detection dual task (S4).

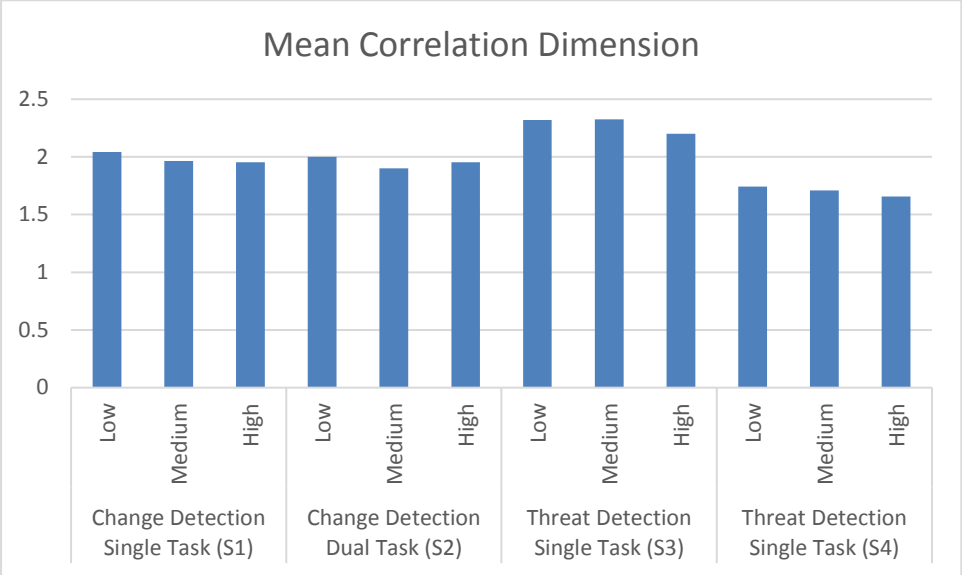

Figure 11 Comparison of correlation dimension for different task levels.

Between the low task level and the medium task level, for the change detection single task, the significant change in correlation dimension was found at central sulcus channel Cz (p-value = 0.013). The marginally significant change was found at left parietal lobe EEG channel P3 (p-value = 0.144). For the change detection dual task, significant change was found at parietal lobe channel Pz (p-value = 0.037). Marginally significant change was found at left central sulcus channel C3 (p-value = 0.108) and left frontal lobe channel F3 (p-value = 0.106). For the threat detection single task, significant change in correlation dimension was found at frontal lobe channel Fz (p-value = 0.015) and left central sulcus channel C3 (p-value = 0.044). The marginally significant change was also found at central sulcus channel Cz (p-value = 0.142) and right central sulcus channel C4 (p-value = 0.098).

On the other hand, between the medium task level and the high task level, significant change in correlation dimension was found in the two threat detection tasks. For the threat detection single task, significant effect was found at frontal lobe channel

Fz (p-value = 0.004) and right frontal lobe channel F4 (p-value = 0.021). Marginally significant effect was also observed at left frontal lobe channel F3 (p-value = 0.057) and parietal lobe channel Pz (p-value = 0.094). For the threat detection dual task, significant effect was found at central sulcus channel Cz (p-value = 0.029). The left parietal lobe channel P3 has marginally significant effect (p-value = 0.117).

Table 49 ANOVA table of correlation dimension for change detection single task (S1) between low and medium level at channel Cz.

Source of Variation	Degrees of Freedom	Sum of Squares	Mean Squares	F	p Value
Scenario	1	7.498	7.498	6.25	0.013
Error	281	337.208	1.200		
Total	282	344.705			

Table 50 ANOVA table of correlation dimension for change detection single task (S1) between low and medium level at channel P3.

Source of Variation	Degrees of Freedom	Sum of Squares	Mean Squares	F	p Value
Scenario	1	2.413	2.413	2.14	0.144
Error	281	316.228	1.125		
Total	282	318.641			

Table 51 ANOVA table of correlation dimension for change detection dual task (S2) between low and medium level at channel C3.

Source of Variation	Degrees of Freedom	Sum of Squares	Mean Squares	F	p Value
Scenario	1	3.081	3.081	2.60	0.108
Error	284	336.039	1.183		
Total	285	339.121			

Table 52 ANOVA table of correlation dimension for change detection dual task (S2) between low and medium level at channel F3.

Source of Variation	Degrees of Freedom	Sum of Squares	Mean Squares	F	p Value
Scenario	1	4.014	4.014	2.63	0.106
Error	284	432.989	1.525		
Total	285	437.003			

Table 53 ANOVA table of correlation dimension for change detection dual task (S2) between low and medium level at channel Pz.

Source of Variation	Degrees of Freedom	Sum of Squares	Mean Squares	F	p Value
Scenario	1	4.999	4.999	4.39	0.037
Error	284	323.160	1.138		
Total	285	328.159			

Table 54 ANOVA table of correlation dimension for threat detection single task (S3) between low and medium level at channel C3.

Source of Variation	Degrees of Freedom	Sum of Squares	Mean Squares	F	p Value
Scenario	1	3.305	3.3052	4.08	0.044
Error	282	228.461	0.8101		
Total	283	231.766			

Table 55 ANOVA table of correlation dimension for threat detection single task (S3) between low and medium level at channel C4.

Source of Variation	Degrees of Freedom	Sum of Squares	Mean Squares	F	p Value
Scenario	1	1.997	1.9970	2.75	0.098
Error	282	204.767	0.7261		
Total	283	206.764			

Table 56 ANOVA table of correlation dimension for threat detection single task (S3) between low and medium level at channel Cz.

Source of Variation	Degrees of Freedom	Sum of Squares	Mean Squares	F	p Value
Scenario	1	1.851	1.8507	2.17	0.142
Error	282	240.288	0.8521		
Total	283	242.139			

Table 57 ANOVA table of correlation dimension for threat detection single task (S3) between low and medium level at channel Fz.

Source of Variation	Degrees of Freedom	Sum of Squares	Mean Squares	F	p Value
Scenario	1	4.516	4.5163	6.05	0.015
Error	282	210.624	0.7469		
Total	283	215.140			

Table 58 ANOVA table of correlation dimension for threat detection single task (S3) between medium and high level at channel F3.

Source of Variation	Degrees of Freedom	Sum of Squares	Mean Squares	F	p Value
Scenario	1	3.550	3.5503	3.66	0.057
Error	283	274.207	0.9689		
Total	284	277.758			

Table 59 ANOVA table of correlation dimension for threat detection single task (S3) between medium and high level at channel F4.

Source of Variation	Degrees of Freedom	Sum of Squares	Mean Squares	F	p Value
Scenario	1	5.475	5.475	5.40	0.021
Error	283	286.774	1.013		
Total	284	292.249			

Table 60 ANOVA table of correlation dimension for threat detection single task (S3) between medium and high level at channel Fz.

Source of Variation	Degrees of Freedom	Sum of Squares	Mean Squares	F	p Value
Scenario	1	6.154	6.1536	8.67	0.004
Error	283	200.851	0.7097		
Total	284	207.005			

Table 61 ANOVA table of correlation dimension for threat detection single task (S3) between medium and high level at channel Pz.

Source of Variation	Degrees of Freedom	Sum of Squares	Mean Squares	F	p Value
Scenario	1	2.051	2.0513	2.82	0.094
Error	283	205.718	0.7269		
Total	284	207.769			

Table 62 ANOVA table of correlation dimension for threat detection dual task (S4) between medium and high level at channel P3.

Source of Variation	Degrees of Freedom	Sum of Squares	Mean Squares	F	p Value
Scenario	1	3.282	3.282	2.47	0.117
Error	282	375.219	1.331		
Total	283	378.502			

5.2.2 Change Detection Tasks Single And Dual Task Scenarios

For the change detection tasks, the dual task only exhibited marginally significant change at the medium task level (p-value = 0.154). At the low task level, the dual task showed significant change in correlation dimension compared to the single task at central sulcus channel Cz (p-value = 0.029) and marginally significant change at left central sulcus channel C3 (p-value = 0.165).

Table 63 Mean correlation dimension for change detection tasks at different task level

Task Level	Scenario	Mean	Grouping	Standard Deviation
Low	Change Detection Single Task (S1)	2.0419	A	1.1245
	Change Detection Dual Task (S2)	2.0006	A	1.1100
Medium	Change Detection Single Task (S1)	1.9641	A	1.1033
	Change Detection Dual Task (S2)	1.9019	A	1.1063
High	Change Detection Single Task (S1)	1.9527	A	1.1032
	Change Detection Dual Task (S2)	1.9523	A	1.1111

Table 64 ANOVA table of correlation dimension for change detection single and dual tasks at medium task level.

Source of Variation	Degrees of Freedom	Sum of Squares	Mean Squares	F	p Value
Scenario	1	2.48	2.481	2.03	0.154
Error	2563	3128.43	1.221		
Total	2564	3130.91			

Table 65 ANOVA table of correlation dimension for change detection tasks at low task level at channel C3.

Source of Variation	Degrees of Freedom	Sum of Squares	Mean Squares	F	p Value
Scenario	1	2.089	2.089	1.94	0.165
Error	282	303.956	1.078		
Total	283	306.045			

Table 66 ANOVA table of correlation dimension for change detection tasks at low task level at channel Cz.

Source of Variation	Degrees of Freedom	Sum of Squares	Mean Squares	F	p Value
Scenario	1	5.757	5.757	4.80	0.029
Error	282	338.512	1.200		
Total	283	344.269			

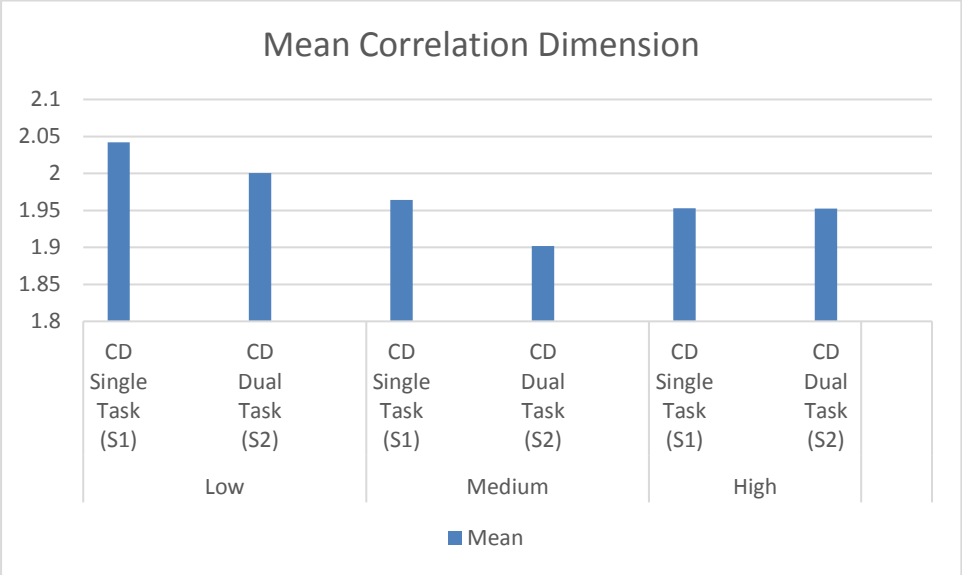

Figure 12 Comparison of correlation dimension for change detection (CD) tasks.

5.2.3 Threat Detection Tasks Single And Dual Task Scenarios

Similar to the results of Lyapunov exponent. Correlation dimension differed significantly at all of the three task levels between the single task scenario and the dual task scenario for the threat detection task (p-value < 0.001). Except for right frontal lobe channel F4 (p-value = 0.100) at low task level and left frontal lobe channel F3 (p-value = 0.071) at high task level, with marginally significant effect, all EEG channels for the dual tasks were significantly different from the single tasks at all three task levels (p-value < 0.05).

Table 67 Mean correlation dimension for threat detection tasks at different task level

Task Level	Scenario	Mean	Grouping	Standard Deviation
Low	Threat Detection Single Task (S3)	2.3188	A	0.9215
	Threat Detection Dual Task (S4)	1.7419	B	1.2123
Medium	Threat Detection Single Task (S3)	2.3253	A	0.8942
	Threat Detection Dual Task (S4)	1.7088	B	1.2073
High	Threat Detection Single Task (S3)	2.0835	A	0.8563
	Threat Detection Dual Task (S4)	1.4229	B	1.0772

Table 68 ANOVA table of correlation dimension for threat detection single and dual tasks at low task level.

Source of Variation	Degrees of Freedom	Sum of Squares	Mean Squares	F	p Value
Scenario	1	211.2	211.180	182.14	0.000
Error	2536	2940.3	1.159		
Total	2537	3151.5			

Table 69 ANOVA table of correlation dimension for threat detection single and dual tasks at medium task level.

Source of Variation	Degrees of Freedom	Sum of Squares	Mean Squares	F	p Value
Scenario	1	243.7	243.694	216.16	0.000
Error	2563	2889.5	1.127		
Total	2564	3133.2			

Table 70 ANOVA table of correlation dimension for threat detection single and dual tasks at high task level.

Source of Variation	Degrees of Freedom	Sum of Squares	Mean Squares	F	p Value
Scenario	1	190.2	190.153	175.92	0.000
Error	2554	2760.6	1.081		
Total	2555	2950.8			

Table 71 ANOVA table of correlation dimension for threat detection tasks at low task level at channel C3.

Source of Variation	Degrees of Freedom	Sum of Squares	Mean Squares	F	p Value
Scenario	1	24.52	24.524	22.62	0.000
Error	280	303.51	1.084		
Total	281	328.03			

Table 72 ANOVA table of correlation dimension for threat detection tasks at low task level at channel C4.

Source of Variation	Degrees of Freedom	Sum of Squares	Mean Squares	F	p Value
Scenario	1	21.84	21.844	18.15	0.000
Error	280	336.92	1.203		
Total	281	358.76			

Table 73 ANOVA table of correlation dimension for threat detection tasks at low task level at channel Cz.

Source of Variation	Degrees of Freedom	Sum of Squares	Mean Squares	F	p Value
Scenario	1	25.36	25.3641	26.85	0.000
Error	280	264.49	0.9446		
Total	281	289.85			

Table 74 ANOVA table of correlation dimension for threat detection tasks at low task level at channel F3.

Source of Variation	Degrees of Freedom	Sum of Squares	Mean Squares	F	p Value
Scenario	1	10.97	10.972	8.97	0.003
Error	280	342.62	1.224		
Total	281	353.59			

Table 75 ANOVA table of correlation dimension for threat detection tasks at low task level at channel F4.

Source of Variation	Degrees of Freedom	Sum of Squares	Mean Squares	F	p Value
Scenario	1	4.532	4.532	2.72	0.100
Error	280	466.224	1.665		
Total	281	470.756			

Table 76 ANOVA table of correlation dimension for threat detection tasks at low task level at channel Fz.

Source of Variation	Degrees of Freedom	Sum of Squares	Mean Squares	F	p Value
Scenario	1	13.85	13.8466	14.24	0.000
Error	280	272.19	0.9721		
Total	281	286.04			

Table 77 ANOVA table of correlation dimension for threat detection tasks at low task level at channel P3.

Source of Variation	Degrees of Freedom	Sum of Squares	Mean Squares	F	p Value
Scenario	1	36.26	36.256	30.17	0.000
Error	280	336.54	1.202		
Total	281	372.80			

Table 78 ANOVA table of correlation dimension for threat detection tasks at low task level at channel P4.

Source of Variation	Degrees of Freedom	Sum of Squares	Mean Squares	F	p Value
Scenario	1	54.51	54.5101	54.52	0.000
Error	280	279.95	0.9998		
Total	281	334.46			

Table 79 ANOVA table of correlation dimension for threat detection tasks at low task level at channel Pz.

Source of Variation	Degrees of Freedom	Sum of Squares	Mean Squares	F	p Value
Scenario	1	40.54	40.5408	41.78	0.000
Error	280	271.72	0.9704		
Total	281	312.26			

Table 80 ANOVA table of correlation dimension for threat detection tasks at medium task level at channel C3.

Source of Variation	Degrees of Freedom	Sum of Squares	Mean Squares	F	p Value
Scenario	1	17.60	17.601	15.15	0.000
Error	283	328.74	1.162		
Total	284	346.34			

Table 81 ANOVA table of correlation dimension for threat detection tasks at medium task level at channel C4.

Source of Variation	Degrees of Freedom	Sum of Squares	Mean Squares	F	p Value
Scenario	1	16.47	16.470	14.96	0.000
Error	283	311.53	1.101		
Total	284	327.99			

Table 82 ANOVA table of correlation dimension for threat detection tasks at medium task level at channel Cz.

Source of Variation	Degrees of Freedom	Sum of Squares	Mean Squares	F	p Value
Scenario	1	27.59	27.588	27.27	0.000
Error	283	286.28	1.012		
Total	284	313.87			

Table 83 ANOVA table of correlation dimension for threat detection tasks at medium task level at channel F3.

Source of Variation	Degrees of Freedom	Sum of Squares	Mean Squares	F	p Value
Scenario	1	11.35	11.351	7.82	0.006
Error	283	411.05	1.452		
Total	284	422.40			

Table 84 ANOVA table of correlation dimension for threat detection tasks at medium task level at channel F4.

Source of Variation	Degrees of Freedom	Sum of Squares	Mean Squares	F	p Value
Scenario	1	15.16	15.157	10.53	0.001
Error	283	407.36	1.439		
Total	284	422.52			

Table 85 ANOVA table of correlation dimension for threat detection tasks at medium task level at channel Fz.

Source of Variation	Degrees of Freedom	Sum of Squares	Mean Squares	F	p Value
Scenario	1	42.54	42.5395	43.48	0.000
Error	283	276.90	0.9784		
Total	284	319.44			

Table 86 ANOVA table of correlation dimension for threat detection tasks at medium task level at channel P3.

Source of Variation	Degrees of Freedom	Sum of Squares	Mean Squares	F	p Value
Scenario	1	31.43	31.429	29.63	0.000
Error	283	300.19	1.061		
Total	284	331.61			

Table 87 ANOVA table of correlation dimension for threat detection tasks at medium task level at channel P4.

Source of Variation	Degrees of Freedom	Sum of Squares	Mean Squares	F	p Value
Scenario	1	62.95	62.9539	68.63	0.000
Error	283	259.61	0.9174		
Total	284	322.57			

Table 88 ANOVA table of correlation dimension for threat detection tasks at medium task level at channel Pz.

Source of Variation	Degrees of Freedom	Sum of Squares	Mean Squares	F	p Value
Scenario	1	36.01	36.0118	39.38	0.000
Error	283	258.77	0.9144		
Total	284	294.78			

Table 89 ANOVA table of correlation dimension for threat detection tasks at high task level at channel C3.

Source of Variation	Degrees of Freedom	Sum of Squares	Mean Squares	F	p Value
Scenario	1	16.04	16.035	13.04	0.000
Error	282	346.87	1.230		
Total	283	362.90			

Table 90 ANOVA table of correlation dimension for threat detection tasks at high task level at channel C4.

Source of Variation	Degrees of Freedom	Sum of Squares	Mean Squares	F	p Value
Scenario	1	24.24	24.237	22.40	0.000
Error	282	305.17	1.082		
Total	283	329.40			

Table 91 ANOVA table of correlation dimension for threat detection tasks at high task level at channel Cz

Source of Variation	Degrees of Freedom	Sum of Squares	Mean Squares	F	p Value
Scenario	1	21.12	21.1168	24.53	0.000
Error	282	242.78	0.8609		
Total	283	263.89			

Table 92 ANOVA table of correlation dimension for threat detection tasks at high task level at channel F3.

Source of Variation	Degrees of Freedom	Sum of Squares	Mean Squares	F	p Value
Scenario	1	4.090	4.090	3.28	0.071
Error	282	351.693	1.247		
Total	283	355.784			

Table 93 ANOVA table of correlation dimension for threat detection tasks at high task level at channel F4.

Source of Variation	Degrees of Freedom	Sum of Squares	Mean Squares	F	p Value
Scenario	1	6.904	6.904	4.82	0.029
Error	282	403.672	1.431		
Total	283	410.575			

Table 94 ANOVA table of correlation dimension for threat detection tasks at high task level at channel Fz.

Source of Variation	Degrees of Freedom	Sum of Squares	Mean Squares	F	p Value
Scenario	1	14.83	14.8318	17.18	0.000
Error	282	243.47	0.8634		
Total	283	258.30			

Table 95 ANOVA table of correlation dimension for threat detection tasks at high task level at channel P3.

Source of Variation	Degrees of Freedom	Sum of Squares	Mean Squares	F	p Value
Scenario	1	43.43	43.4345	46.49	0.000
Error	282	263.48	0.9343		
Total	283	306.9			

Table 96 ANOVA table of correlation dimension for threat detection tasks at high task level at channel P4.

Source of Variation	Degrees of Freedom	Sum of Squares	Mean Squares	F	p Value
Scenario	1	51.66	51.663	51.16	0.000
Error	282	284.79	1.010		
Total	283	336.45			

Table 97 ANOVA table of correlation dimension for threat detection tasks at high task level at channel Pz.

Source of Variation	Degrees of Freedom	Sum of Squares	Mean Squares	F	p Value
Scenario	1	30.99	30.9867	32.73	0.000
Error	282	267.00	0.9468		
Total	283	297.99			

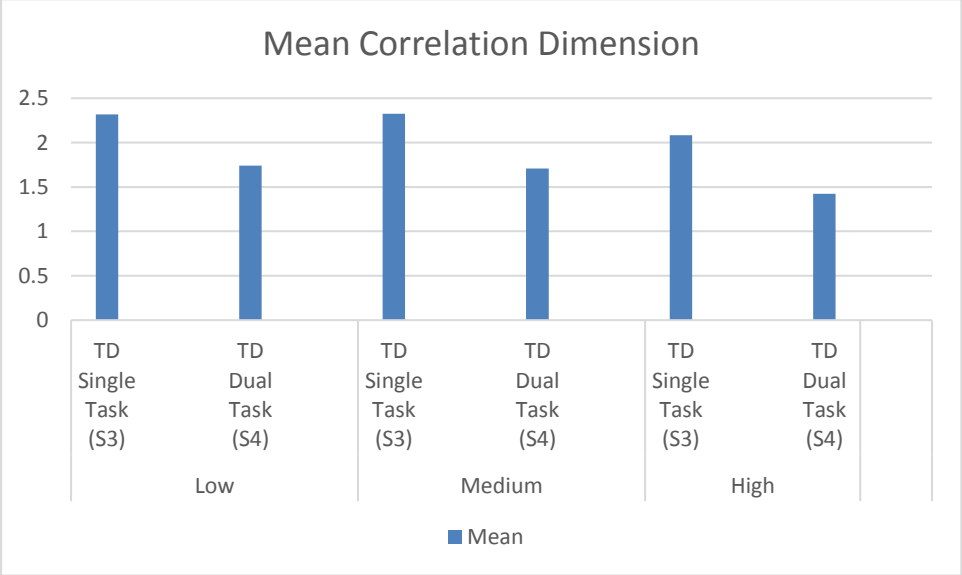

Figure 13 Comparison of correlation dimension for threat detection (TD) tasks.

5.3 0-1 Test

5.3.1 Task Levels

The computation results of the 0-1 test, which is the values of k-median, are close to 1 for each task level and for each EEG channel, and thus indicating the existence of chaotic dynamics in EEG data. According to the results of one-way ANOVA, between the low task level and the medium task level, change detection dual task showed significant change of nonlinearity (p-value = 0.037). Marginally significant change was found for threat detection dual task (p-value = 1.59). When the task level rises from medium level to high level, the change detection single task showed significant effect (p-value = 0.027). The threat detection single task showed marginally significant effect (p-value = 0.096).

Furthermore, when the task level increases from low level to medium level, for the change detection single task, marginally significant change in nonlinearity was found at right parietal lobe channel P4 (p-value = 0.060). For the change detection dual task, significant change was found at left frontal lobe channel F3 (p-value = 0.030), and right central sulcus channel C4 (p-value = 0.037). Marginally significant change was found at frontal lobe channel Fz (p-value = 0.175). For the threat detection single task, marginally significant effect was observed at left frontal lobe channel F3 (p-value = 0.165), left central sulcus channel C3 (p-value = 0.109), and central sulcus channel Cz (p-value = 0.094). The significant effect was also found at right central lobe channel C4 for the threat detection dual task (p-value = 0.032), along with marginally significant

effect at parietal lobe channel Pz (p-value = 0.082).

When the task level shifts from medium level to high level, for the change detection single task, significant change was found at right frontal lobe channel F4 (p-value = 0.043). Marginally change was found at parietal lobe channels Pz (p-value = 0.107) and P4 (p-value = 0.091). For the change detection dual task, marginally significant change was observed at left central lobe channel C3 (p-value = 0.064) and right parietal lobe P4 (p-value = 0.116). The threat detection single task showed significant effect at parietal lobe channel Pz (p-value = 0.160). Additionally, the threat detection dual task showed significant change at parietal lobe channel Pz (p-value = 0.010) and marginally significant change at left parietal lobe channel P3 (p-value = 0.114).

Table 98 Comparison of 0-1 test for different task levels

Scenario	Task Level	Mean	Grouping	Standard Deviation
Change Detection Single Task (S1)	Low	0.98246	A	0.04059
	Medium	0.98371	A	0.03870
	High	0.97988	B	0.04848
Change Detection Dual Task (S2)	Low	0.984650	A	0.034497
	Medium	0.98155	B	0.04082
	High	0.98185	B	0.05371
Threat Detection Single Task (S3)	Low	0.98517	A	0.03773
	Medium	0.986581	A	0.028678
	High	0.98440	A	0.03723
Threat Detection Dual Task (S4)	Low	0.98401	A	0.03909
	Medium	0.98131	A	0.05610
	High	0.98297	A	0.03884

Table 99 ANOVA table of 0-1 test for change detection single task (S1) between medium and high level.

Source of Variation	Degrees of Freedom	Sum of Squares	Mean Squares	F	p Value
Task Level	1	0.00936	0.009361	4.87	0.027
Error	2554	4.91397	0.001924		
Total	2555	4.92333			

Table 100 ANOVA table of 0-1 test for change detection dual task (S2) between low and medium level.

Source of Variation	Degrees of Freedom	Sum of Squares	Mean Squares	F	p Value
Task Level	1	0.00619	0.006191	4.33	0.037
Error	2572	3.67323	0.001428		
Total	2573	3.67942			

Table 101 ANOVA table of 0-1 test for threat detection single task (S3) between medium and high level.

Source of Variation	Degrees of Freedom	Sum of Squares	Mean Squares	F	p Value
Task Level	1	0.00305	0.001273	2.77	0.096
Error	2563	2.82765	0.001121		
Total	2564	2.83070			

Table 102 ANOVA table of 0-1 test for threat detection dual task (S4) between low and medium level.

Source of Variation	Degrees of Freedom	Sum of Squares	Mean Squares	F	p Value
Task Level	1	0.00466	0.004657	1.99	0.159
Error	2545	5.95683	0.002341		
Total	2546	5.96149			

Table 103 ANOVA table of 0-1 test for change detection single task (S1) between low and medium level at channel P4.

Source of Variation	Degrees of Freedom	Sum of Squares	Mean Squares	F	p Value
Scenario	1	0.002916	0.002916	3.56	0.060
Error	281	0.230277	0.000819		
Total	282	0.233193			

Table 104 ANOVA table of 0-1 test for change detection dual task (S2) between low and medium level at channel C4.

Source of Variation	Degrees of Freedom	Sum of Squares	Mean Squares	F	p Value
Scenario	1	0.003315	0.003315	4.40	0.037
Error	284	0.214062	0.000754		
Total	285	0.217377			

Table 105 ANOVA table of 0-1 test for change detection dual task (S2) between low and medium level at channel F3.

Source of Variation	Degrees of Freedom	Sum of Squares	Mean Squares	F	p Value
Scenario	1	0.005163	0.005163	4.77	0.030
Error	284	0.307387	0.001082		
Total	285	0.312550			

Table 106 ANOVA table of 0-1 test for change detection dual task (S2) between low and medium level at channel Fz.

Source of Variation	Degrees of Freedom	Sum of Squares	Mean Squares	F	p Value
Scenario	1	0.004350	0.004350	1.85	0.175
Error	284	0.666842	0.002348		
Total	285	0.671192			

Table 107 ANOVA table of 0-1 test for threat detection single task (S3) between low and medium level at channel C3.

Source of Variation	Degrees of Freedom	Sum of Squares	Mean Squares	F	p Value
Scenario	1	0.001489	0.001489	2.58	0.109
Error	282	0.162487	0.000576		
Total	283	0.163976			

Table 108 ANOVA table of 0-1 test for threat detection single task (S3) between low and medium level at channel Cz.

Source of Variation	Degrees of Freedom	Sum of Squares	Mean Squares	F	p Value
Scenario	1	0.004841	0.004841	2.82	0.094
Error	282	0.483844	0.001716		
Total	283	0.488684			

Table 109 ANOVA table of 0-1 test for threat detection single task (S3) between low and medium level at channel F3.

Source of Variation	Degrees of Freedom	Sum of Squares	Mean Squares	F	p Value
Scenario	1	0.000608	0.000608	1.94	0.165
Error	282	0.088410	0.000314		
Total	283	0.089018			

Table 110 ANOVA table of 0-1 test for threat detection dual task (S4) between low and medium level at channel C4.

Source of Variation	Degrees of Freedom	Sum of Squares	Mean Squares	F	p Value
Scenario	1	0.006424	0.006424	4.64	0.032
Error	281	0.388859	0.001384		
Total	282	0.395282			

Table 111 ANOVA table of 0-1 test for threat detection dual task (S4) between low and medium level at channel Pz.

Source of Variation	Degrees of Freedom	Sum of Squares	Mean Squares	F	p Value
Scenario	1	0.002897	0.002897	3.04	0.082
Error	281	0.267456	0.000952		
Total	282	0.270354			

Table 112 ANOVA table of 0-1 test for change detection single task (S1) between medium and high level at channel F4.

Source of Variation	Degrees of Freedom	Sum of Squares	Mean Squares	F	p Value
Scenario	1	0.002853	0.002853	4.15	0.043
Error	282	0.193987	0.000688		
Total	283	0.196840			

Table 113 ANOVA table of 0-1 test for change detection single task (S1) between medium and high level at channel P4.

Source of Variation	Degrees of Freedom	Sum of Squares	Mean Squares	F	p Value
Scenario	1	0.003107	0.003107	2.87	0.091
Error	282	0.305015	0.001082		
Total	283	0.308122			

Table 114 ANOVA table of 0-1 test for change detection single task (S1) between medium and high level at channel Pz.

Source of Variation	Degrees of Freedom	Sum of Squares	Mean Squares	F	p Value
Scenario	1	0.004725	0.004725	2.62	0.107
Error	282	0.509389	0.001806		
Total	283	0.514114			

Table 115 ANOVA table of 0-1 test for change detection dual task (S2) between medium and high level at channel C3.

Source of Variation	Degrees of Freedom	Sum of Squares	Mean Squares	F	p Value
Scenario	1	0.004465	0.004465	3.47	0.064
Error	284	0.365664	0.001288		
Total	285	0.370129			

Table 116 ANOVA table of 0-1 test for change detection dual task (S2) between medium and high level at channel P4.

Source of Variation	Degrees of Freedom	Sum of Squares	Mean Squares	F	p Value
Scenario	1	0.001968	0.001968	2.48	0.116
Error	284	0.225489	0.000794		
Total	285	0.227457			

Table 117 ANOVA table of 0-1 test for threat detection single task (S3) between medium and high level at channel Pz.

Source of Variation	Degrees of Freedom	Sum of Squares	Mean Squares	F	p Value
Scenario	1	0.003257	0.003257	1.98	0.160
Error	283	0.465012	0.001643		
Total	284	0.468268			

Table 118 ANOVA table of 0-1 test for threat detection dual task (S4) between medium and high level at channel P3.

Source of Variation	Degrees of Freedom	Sum of Squares	Mean Squares	F	p Value
Scenario	1	0.002472	0.002472	2.51	0.114
Error	282	0.277823	0.000985		
Total	283	0.280296			

Table 119 ANOVA table of 0-1 test for threat detection dual task (S4) between medium and high level at channel Pz.

Source of Variation	Degrees of Freedom	Sum of Squares	Mean Squares	F	p Value
Scenario	1	0.006043	0.006043	6.75	0.010
Error	282	0.252561	0.000896		
Total	283	0.258604			

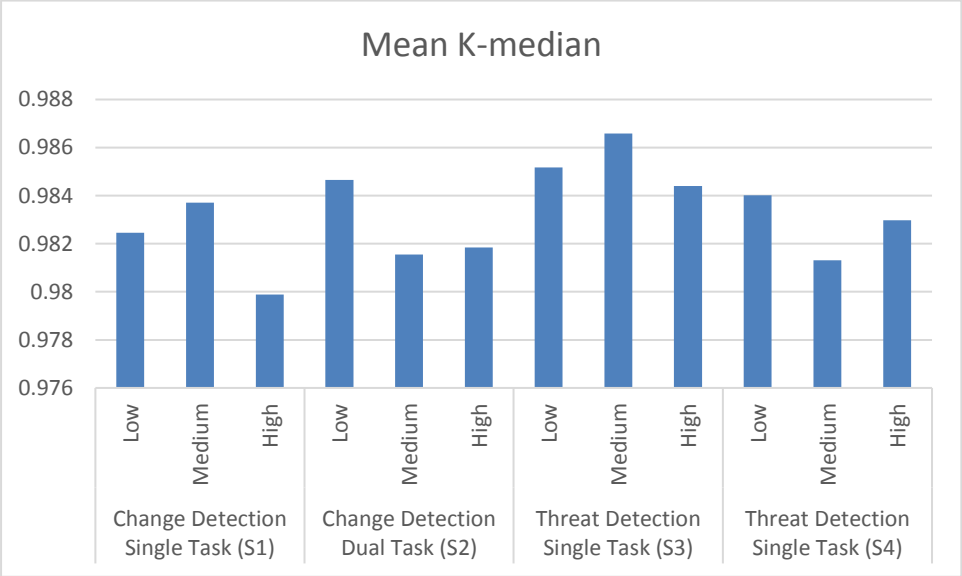

Figure 14 Comparison of K-median from 0-1 test for different task levels.

5.3.2 Change Detection Tasks Single And Dual Task Scenarios

For the change detection tasks, the dual task showed marginally significant change at the low task level (p-value = 0.141) and the medium task level (p-value = 0.169). At the low task level, there was marginally significant change observed at frontal lobe channel Fz (p-value = 0.123) for the dual task. At the medium task level, marginally significant change between the dual task and the single task was found at right parietal lobe channel P4 (p-value = 0.0176). At the high task level, the dual task differed marginally significantly at parietal lobe, including channel P3 (p-value =

0.098), Pz (p-value = 0.124), and P4 (p-value = 0.127).

Table 120 Mean K-median for change detection tasks at different task level

Task Level	Scenario	Mean	Grouping	Standard Deviation
Low	Change Detection Single Task (S1)	0.98246	A	0.04059
	Change Detection Dual Task (S2)	0.984650	A	0.034497
Medium	Change Detection Single Task (S1)	0.98371	A	0.03870
	Change Detection Dual Task (S2)	0.98155	A	0.04082
High	Change Detection Single Task (S1)	0.97988	A	0.04848
	Change Detection Dual Task (S2)	0.98185	A	0.05371

Table 121 ANOVA table of 0-1 test for change detection single and dual tasks at low task level.

Source of Variation	Degrees of Freedom	Sum of Squares	Mean Squares	F	p Value
Scenarios	1	0.00307	0.003069	2.17	0.141
Error	2554	3.61916	0.001417		
Total	2555	3.62223			

Table 122 ANOVA table of 0-1 test for change detection single and dual tasks at medium task level.

Source of Variation	Degrees of Freedom	Sum of Squares	Mean Squares	F	p Value
Scenarios	1	0.00299	0.002990	1.89	0.169
Error	2563	4.05582	0.001582		
Total	2564	4.05881			

Table 123 ANOVA table of 0-1 test for change detection tasks at low task level at channel Fz.

Source of Variation	Degrees of Freedom	Sum of Squares	Mean Squares	F	p Value
Scenario	1	0.007163	0.007163	2.39	0.123
Error	282	0.845300	0.002998		
Total	283	0.852464			

Table 124 ANOVA table of 0-1 test for change detection tasks at medium task level at channel P4.

Source of Variation	Degrees of Freedom	Sum of Squares	Mean Squares	F	p Value
Scenario	1	0.002399	0.002399	3.18	0.076
Error	283	0.213851	0.000756		
Total	284	0.216250			

Table 125 ANOVA table of 0-1 test for change detection tasks at high task level at channel P3.

Source of Variation	Degrees of Freedom	Sum of Squares	Mean Squares	F	p Value
Scenario	1	0.005843	0.005843	2.76	0.098
Error	283	0.598960	0.002116		
Total	284	0.604803			

Table 126 ANOVA table of 0-1 test for change detection tasks at high task level at channel P4.

Source of Variation	Degrees of Freedom	Sum of Squares	Mean Squares	F	p Value
Scenario	1	0.002615	0.002615	2.34	0.127
Error	283	0.316654	0.001119		
Total	284	0.319269			

Table 127 ANOVA table of 0-1 test for change detection tasks at high task level at channel Pz.

Source of Variation	Degrees of Freedom	Sum of Squares	Mean Squares	F	p Value
Scenario	1	0.003849	0.003849	2.38	0.124
Error	283	0.457502	0.001617		
Total	284	0.461352			

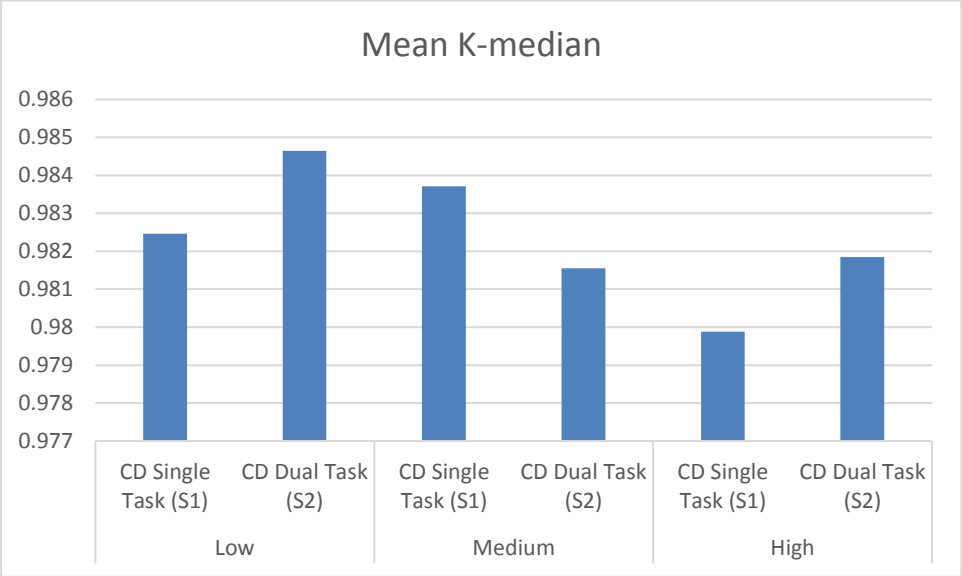

Figure 15 Comparison of the results of 0-1 test for change detection (CD) tasks.

5.3.3 Threat Detection Tasks Single And Dual Task Scenarios

The result of 0-1 test changed significantly at the medium task level between the single task scenario and the dual task scenario for the threat detection task (p-value = 0.003). For the threat detection tasks, at the low task level, the dual task was found marginally significantly different from the single task at left frontal lobe channel F3 (p-value = 0.120). At the medium task level, the dual task changed marginally significantly at frontal lobe channel Fz (p-value = 0.117) and left central sulcus channel C3 (p-value = 0.140). At the high task level, the dual task also showed marginally significant change from the single task, located at left frontal lobe channel F3 (p-value = 0.127) and left

parietal lobe channel P3 (p-value = 0.109).

Table 128 Mean K-median for threat detection tasks at different task level

Task Level	Scenario	Mean	Grouping	Standard Deviation
Low	Threat Detection Single Task (S3)	0.98517	A	0.03773
	Threat Detection Dual Task (S4)	0.98401	A	0.03909
Medium	Threat Detection Single Task (S3)	0.986581	A	0.028678
	Threat Detection Dual Task (S4)	0.98131	B	0.05610
High	Threat Detection Single Task (S3)	0.98440	A	0.03723
	Threat Detection Dual Task (S4)	0.98297	A	0.03884

Table 129 ANOVA table of 0-1 test for threat detection single and dual tasks at medium task level.

Source of Variation	Degrees of Freedom	Sum of Squares	Mean Squares	F	p Value
Scenarios	1	0.01783	0.017827	9.00	0.003
Error	2563	5.07697	0.001981		
Total	2564	5.09479			

Table 130 ANOVA table of 0-1 test for threat detection tasks at low task level at channel F3.

Source of Variation	Degrees of Freedom	Sum of Squares	Mean Squares	F	p Value
Scenario	1	0.001972	0.001972	2.43	0.120
Error	280	0.226826	0.000810		
Total	281	0.228797			

Table 131 ANOVA table of 0-1 test for threat detection tasks at medium task level at channel C3.

Source of Variation	Degrees of Freedom	Sum of Squares	Mean Squares	F	p Value
Scenario	1	0.000856	0.000856	2.19	0.140
Error	283	0.110679	0.000391		
Total	284	0.111536			

Table 132 ANOVA table of 0-1 test for threat detection tasks at medium task level at channel Fz.

Source of Variation	Degrees of Freedom	Sum of Squares	Mean Squares	F	p Value
Scenario	1	0.01280	0.012804	2.47	0.117
Error	283	1.46689	0.005183		
Total	284	1.47969			

Table 133 ANOVA table of 0-1 test for threat detection tasks at high task level at channel F3.

Source of Variation	Degrees of Freedom	Sum of Squares	Mean Squares	F	p Value
Scenario	1	0.003636	0.003636	2.34	0.127
Error	282	0.438341	0.001554		
Total	283	0.441977			

Table 134 ANOVA table of 0-1 test for threat detection tasks at high task level at channel P3.

Source of Variation	Degrees of Freedom	Sum of Squares	Mean Squares	F	p Value
Scenario	1	0.002798	0.002798	2.58	0.109
Error	282	0.305490	0.001083		
Total	283	0.308288			

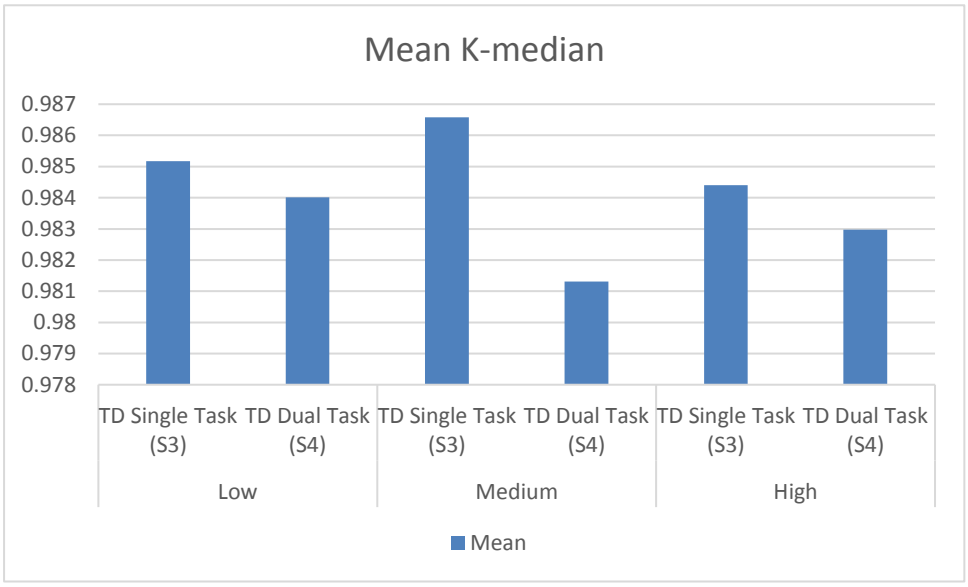

Figure 16 Comparison of the results of 0-1 test for threat detection (TD) tasks.

CHAPTER 6: CONCLUSION AND DISCUSSION

The goal of this study was to distinguish the variations of mental workload by examining brain activity using nonlinear dynamics of EEG. By examining several nonlinear dynamics algorithm, the results elicited from this study first verified the existence of the chaotic dynamics in the EEG time series. The largest Lyapunov exponents are positive values. The correlation dimension and the embedding phase space of EEG time series are saturated. The results of 0-1 test are close to 1.

Furthermore, this study supported the hypothesis that EEG data exhibits a change in the level of nonlinearity corresponding to differed task levels. The nonlinear analysis of EEG time series data is able to discriminate the change in brain activity derived from the changes in task load. All nonlinear dynamics analysis techniques used in this study is able to find the difference of nonlinearity in EEG among task levels, as well as between single task scenario and dual task scenario.

Correlation dimension has finite values when the system is deterministic but not completely random, thus is a suitable metric to evaluate the nonlinear dynamics of the system. In the process of phase space reconstruction, it is crucial to select appropriate parameters time lag and embedding dimension. A time lag that is too small will cause the phase space reconstruction to have the nearly same value and therefore lead to redundancy. On the other hand, a time lag that is too big will result in unrelated embedding vectors. The objective of determining time lag is to find the appropriate

expansion of embedding vectors in the phase space. Also, if the embedding dimension is too small, the attractor will not completely unfold. However, if the embedding dimension is too big, the system will be close to noise. The principle for determination of embedding dimension states that the embedding dimension is larger than two times of correlation dimension (m>2D). But the drawback is that the value of the correlation dimension must be determined in advance. Previously, researchers achieve the right value of embedding dimension by repetitive calculation of correlation dimension with the different assumption of embedding dimension until the criterion is reached. However, the calculation is difficult because the calculation depends on time lag also. In this study, the false nearest neighbor method was employed in order to insure that the attractors are completely unfolded. The false nearest neighbor method looks for the nearest neighbors in the phase space that remain close when the embedding dimension increases (Quiroga, 2002).

The EEG data obtained from the experiment that was used in this study was analyzed by numerous preliminary studies using traditional power spectral analysis. For instance, Mathews et al (2017) suggested the correlations between EEG band spectral power and subjective measures, higher distress was found in accordance with higher beta and theta power. However, the variations among EEG channels were not the focus. Mathews et al (2011) also suggested that physiological was more effective than subjective measures. Teo et al (2015) suggest that the physiological measures were sensitive enough to distinguish the difference in workload. The physiological measures were more sensitive for the change detection tasks than the threat detection tasks. Teo

et al (2018) confirmed that the dual tasks had increased mental workload as well as decreased task performance. Teo et al (2017) found that theta power and correct percentage had a negative correlation for the change detection tasks. Abich et al (2013) investigated the mental workload through eye fixation. The number of eye fixations increased as task difficulty increased. As to the fixation duration for different task scenarios, the threat detection was concluded to have a higher demand for focal vision. However, the correlation was unconcluded because the duration decreased from low demand level to medium level. Matthews et al (2015) also found that different psychophysiological measures were sensitive to each workload manipulation, but not to both tasks at the same time. Different physiological measures showed varied performance for different types of workload manipulation. EEG was effective in regarding with differentiating dual task from single task. EEG frontal theta power was sensitive to the threat detection tasks and the single task change detection. EEG alpha power was not sensitive to the change in different task types. Talor et al (2015) found that EEG alpha power in occipital lobe increased at the higher task level. Moreover, EEG beta power in frontal lobe and occipital lobe decreased under lower task demand. In the study by Reinerman-Jones et al (2014), the frontal theta power evidently showed that the single threat detection task had lower mental workload compared to the single change detection tasks and the dual tasks. Besides, the single change detection task could not distinguish from the dual tasks. Frontal theta power was able to discriminate change of mental workload between the single change detection tasks and single threat detection tasks, but not between the single threat detection tasks and the dual tasks. The

EEG beta power showed that mental workload was the highest for single threat detection task. Abich et al (2015) found that the EEG beta power was relatively high for frontal beta power in the resting baseline condition, and was lower for the change detection tasks. The low frontal theta power was able to effectively predict the task performance for the change detection tasks. Frontal alpha, beta, and theta power had positive correlation with the distress generated during performing the task. There was no statistical significance found in the threat detection tasks. The nonlinear analysis methodologies used in this study provide a new way to quantify brain activity, serves as a useful method for computation of cross correlations among EEG channels and visualization of the intricate dynamics of EEG.

Among the three methods applied in this study, the nonlinear dynamics analysis methods succeeded in detecting the existence of nonlinearity in different brain activity levels. They are able to demonstrate the change in nonlinearity in accordance with the difficulty of the task scenarios. The 0-1 test is more efficient regarding calculation and is easier to code and debug. Moreover, this research obtained new insights from the psychophysiological mental workload measurement used in the preliminary study.

Moreover, it is recommended to examine the EEG time series for each EEG channel individually rather than just estimating at a general level. The brain activity in certain brain areas sometimes is complicated. Thus the activity in these particular channels might not be reflected when estimate using the work level as a whole.

The significant change in nonlinearity in EEG channels observed in this study is consistent with many an experimental observation that the frontal lobe and the parietal

lobe become more activated with the increased task demands for visual detection tasks. Although the parietal lobe is considered as an important role in spatial processing and visual attention (Kanwisher and Wojciulik, 2000), various activities in the frontal lobe are found when subjects try to shift their visual attention, rather than holding the attention at a fixed target. The activity in superior parietal lobe (SPL) areas also increase during attention shifts (Coull and Nobre, 1998; Corbetta et al, 1998; Culham et al, 1998; Nobre et al, 2000). These areas related to attention shifts include the intraparietal sulcus (IPS), superior frontal lobe areas, such as the frontal eye fields (FEF), on the sides of frontal lobe, such as channel F3 and F4, the supplementary eye field (SEF), and the supplementary motor area (SMA), near central sulcus area, channel C4. SPL and IPS are especially more active when the targets of the visual detection tasks are presented in alternating colors or shapes (Le et al, 1998). Besides, the temporoparietal junction (TPJ) becomes more activated in visual detection tasks in which the stimulus has changing frequencies. Besides, the brain is more activated in the right hemisphere for visual attention at changing targets (Corbetta and Shulman, 2002).

CHAPTER 7: FUTURE RESEARCH

For future research, it is necessary to maintain the conditions of the experiment in a relatively high level of control, for both during task condition and resting condition. There is an overlap in activated brain areas for visual attention and auditory attention, or even tactile attention. Additionally, auditory attention causes more activations in the inferior frontal lobe and the inferior parietal lobe (Klinberg, 1998; Tzourio et al, 1997). Spatially directed tactile attention can enhance the activation in the same intraparietal areas as the visual attention (Banati et al, 2000, Burton et al, 1999; Hadjikhani and Roland, 1998). Furthermore, TPJ is more activated when the stimulus is presented as a changing rate, no matter the sensory modality, such as visual, auditory, or tactile (Downar et al, 2000). The locations of activation and the level of brain activity can be easily altered by the distraction caused by multiple sensory modalities, and thus influence the result of the research.

It is also necessary to control the duration of the experiment, in order to better differentiate the arousal of brain areas caused by a higher level of workload and the activity change caused by long-term fatigue.

Future studies might also consider including more EEG channel locations when investigating the nonlinearity of EEG time series, in order to obtain a more complete, more detailed, and more realistic depiction of the effect of mental workload on the change of brain activity. The nonlinear analysis of EEG has a wide range of application. It can also be able to use for examining the effect of mental workload that is generated

from sensory modalities other than visual attention. The nonlinear analysis of EEG is suitable to investigate a variety of more sophisticated tasks, including but not limited to, auditory perception, memory tasks, visual perception with informative input, logical thinking, or even the effect of emotion change on task. Therefore, nonlinear analysis is an efficient tool for obtaining a more profound understanding of the influence of mental workload on the human brain.

LIST OF REFERENCES

Abich, J., IV, Reinerman-Jones, L., & Taylor, G. S. (2013). Investigating workload measures for adaptive training systems. In Proceedings of the Human Factors and Ergonomics Society Annual Meeting(Vol. 57, No. 1, pp. 2091-2095). SAGE Publications.

Abich, J., IV, Matthew, G., & Reinerman-Jones, L. (2015). Individual differences in UGV operation: A comparison of subjective and psychophysiological predictors. In Proceedings of the Human Factors and Ergonomics Society Annual Meeting (Vol. 59, No. 1, pp. 741-745). SAGE Publications.

Aftanas, L. I., Lotova, N. V., Koshkarov, V. I., Makhnev, V. P., Mordvintsev, Y. N., & Popov, S. A. (1998). Non-linear dynamic complexity of the human EEG during evoked emotions. International Journal of Psychophysiology,28(1), 63-76.

Ascani, F., Keeler, P., Kubiak, R., Laney, S., Musuvathy, S., & Papo, D. (2008). Detection of low-dimensional chaos in quasi-periodic time series: The 0-1 Test. Tech. Rep., Santa Fe Institute Complex Systems Summer School.

Azarnoosh, M., Nasrabadi, A. M., & Mohammadi, M. R. (2011). Investigation of mental fatigue through EEG signal processing based on nonlinear analysis: symbolic dynamics. Chaos, Solitons and Fractals, 44(12), 1054-1062.

Balagué, N., Hristovski, R., Aragonés, D., & Tenenbaum, G. (2012). Nonlinear model of attention focus during accumulated effort. Psychology of Sport and Exercise, 13(5), 591-597.

Banati, R. B., Goerres, G. W., Tjoa, C., Aggleton, J. P., & Grasby, P. (2000). The functional anatomy of visual-tactile integration in man: a study using positron emission tomography. Neuropsychologia, 38(2), 115-124.

Beatty, J. (1976). Pupillometric measurement of cognitive workload. Proceedings of the Twelfth Annual Conference on Manual Control, NASA TMX-73, 170.

Berka, C., Levendowski, D. J., Lumicao, M. N., Yau, A., Davis, G., Zivkovic, V. T., ... & Craven, P. L. (2007). EEG correlates of task engagement and mental workload in vigilance, learning, and memory tasks. Aviation, space, and environmental medicine, 78(5), B231-B244.

Borghini, G., Vecchiato, G., Toppi, J., Astolfi, L., Maglione, A., Isabella, R., ... & Polidori, L. (2012, August). Assessment of mental fatigue during car driving by using high resolution EEG activity and neurophysiologic indices. In 2012 Annual International Conference of the IEEE Engineering in Medicine and Biology Society (pp. 6442-6445). IEEE.

Brooking, J. B., Wilsonh, G. F., & Swain, C. R. (1996). Psychophysiological responses to changes in workload during simulated air traffic control. Biological Psychology, 42(3), 361-377.

Brouwer, A. M., Hogervorst, M. A., Van Erp, J. B., Heffelaar, T., Zimmerman, P. H., & Oostenveld, R. (2012). Estimating workload using EEG spectral power and ERPs in the n-back task. Journal of neural engineering, 9(4), 045008.

Budhraja, M., Kumar, N., & Saha, L. M. (2012). The 0-1 test applied to Peter-De-Jong Map. International Journal of Engineering and Innovative Technology (IJEIT),

2(6).

Burton, H., Abend, N. S., MacLeod, A. M., Sinclair, R. J., Snyder, A. Z., & Raichle, M. E. (1999). Tactile attention tasks enhance activation in somatosensory regions of parietal cortex: a positron emission tomography study. Cerebral Cortex, 9(7), 662-674.

Cao, L. (1997). Practical method for determining the minimum embedding dimension of a scalar time series. Physica D: Nonlinear Phenomena, 110(1-2), 43-50.

Carroll, D., Turner, J. R., & Hellawell, J. C. (1986). Heart rate and oxygen consumption during active psychological challenge: the effects of level of difficulty. Psychophysiology, 23(2), 174-181.

Chaouachi, M., Jraidi, I., & Frasson, C. (2011, July). Modeling mental workload using EEG features for intelligent systems. In International Conference on User Modeling, Adaptation, and Personalization (pp. 50-61). Springer, Berlin, Heidelberg.

Chelidze, D. (2017). Reliable Estimation of Minimum Embedding Dimension Through Statistical Analysis of Nearest Neighbors. Journal of Computational and Nonlinear Dynamics, 12(5), 051024.

Chowdhury, D. R., Iyengar, A. N. S., & Lahiri, S. (2012). Gottwald Melborune (0-1) test for chaos in a plasma. Nonlinear Processes in Geophysics, 19(1), 53-56.

Clark, V. P., Fannon, S., Lai, S., Benson, R., & Bauer, L. (2000). Responses to rare visual target and distractor stimuli using event-related fMRI. Journal of Neurophysiology, 83(5), 3133-3139.

Cooper, J. M., Medeiros-Ward, N., & Strayer, D. L. (2013). The impact of eye movements and cognitive workload on lateral position variability in driving. Human Factors: The Journal of the Human Factors and Ergonomics Society, 0018720813480177.

Corbetta, M., Akbudak, E., Conturo, T. E., Snyder, A. Z., Ollinger, J. M., Drury, H. A., ... & Shulman, G. L. (1998). A common network of functional areas for attention and eye movements. Neuron, 21(4), 761-773.

Corbetta, M., & Shulman, G. L. (2002). Control of goal-directed and stimulus-driven attention in the brain. Nature reviews neuroscience, 3(3), 201.

Coull, J. T., & Nobre, A. C. (1998). Where and when to pay attention: the neural systems for directing attention to spatial locations and to time intervals as revealed by both PET and fMRI. Journal of Neuroscience, 18(18), 7426-7435.

Culham, J. C., Brandt, S. A., Cavanagh, P., Kanwisher, N. G., Dale, A. M., & Tootell, R. B. (1998). Cortical fMRI activation produced by attentive tracking of moving targets. Journal of neurophysiology, 80(5), 2657-2670.

Dawes, J. H. P., & Freeland, M. C. (2008). The '0–1 test for chaos' and strange nonchaotic attractors. Retrieved from http://people.bath.ac.uk/jhpd20/ publications/sna.pdf

Di Stasi, L. L., Antolí, A., Gea, M., & Cañas, J. J. (2011). A neuroergonomic approach to evaluating mental workload in hypermedia interactions.International Journal of Industrial Ergonomics, 41(3), 298-304.

Díaz, M. H., Córdova, F. M., Cañete, L., Palominos, F., Cifuentes, F., Sánchez, C., &

Herrera, M. (2015). Order and chaos in the brain: fractal time series analysis of the EEG activity during a cognitive problem solving task.Procedia Computer Science, 55, 1410-1419.

Downar, J., Crawley, A. P., Mikulis, D. J., & Davis, K. D. (2000). A multimodal cortical network for the detection of changes in the sensory environment. Nature neuroscience, 3(3), 277.

Downar, J., Crawley, A. P., Mikulis, D. J., & Davis, K. D. (2001). The effect of task relevance on the cortical response to changes in visual and auditory stimuli: an event-related fMRI study. Neuroimage, 14(6), 1256-1267.

Dunkel, J. (1990, June). On the modeling of workload dependent memory faults. In Fault-Tolerant Computing, 1990. FTCS-20. Digest of Papers., 20th International Symposium (pp. 348-355). IEEE.

Earle, J. B. B., & Pikus, A. (1982). The effect of sex and task difficulty on EEG alpha activity in association with arithmetic. Biological Psychology, 15(1-2), I-14.

Elizabeth'C, H., Murphy, B., Rajmohan, R., Anderson, R. C., Baker, M., Zupancic, S., ... & Richman, D. (2016). Visual, Auditory, and Cross Modal Sensory Processing in Adults with Autism: An EEG Power and BOLD fMRI Investigation. Frontiers in human neuroscience, 10.

Falconer, I., Gottwald, G. A., Melbourne, I., & Wormnes, K. (2007). Application of the 0-1 test for chaos to experimental data. SIAM Journal on Applied Dynamical Systems, 6(2), 395-402.

Galy, E., Cariou, M., & Mélan, C. (2012). What is the relationship between mental

workload factors & cognitive load types?. International Journal of Psychophysiology, 83(3), 269-275.

Gevins, A., Smith, M. E., Leong, H., McEvoy, L., Whitfield, S., Du, R., & Rush, G. (1998). Monitoring working memory load during computer-based tasks with EEG pattern recognition methods. Human factors, 40(1), 79-91.

Gielo-Perczak, K., Karwowski, W., & Rodrick, D. (2009). Nonlinear behavior of the center of pressure in simulated standing on elevated construction beams. Work, 34(2), 195-203.

Gottwald, G. A., & Melbourne, I. (2003). A new test for chaos in deterministic systems. Proceedings: Mathematical, Physical and Engineering Sciences, 460(2042), 603-611.

Gottwald, G. A., & Melbourne, I. (2005). Testing for chaos in deterministic systems with noise. Physica D: Nonlinear Phenomena, 212(1), 100-110.

Grassberger, P., & Procaccia, I. (1983). Characterization of strange attractors. Physical review letters, 50(5), 346.

Guastello, S. J. (2001). Nonlinear dynamics in psychology. Discrete Dynamics in Nature and Society, 6(1), 11-29.

Guastello, S. J. (2010). Nonlinear dynamics of team performance and adaptability in emergency response. Human Factors: The Journal of the Human Factors and Ergonomics Society, 52(2), 162-172.

Guastello, S. J., Boeh, H., Schimmels, M., Gorin, H., Huschen, S., Davis, E., ... & Poston, K. (2012). Cusp catastrophe models for cognitive workload and fatigue

in a verbally cued pictorial memory task. Human factors, 54(5), 811-825.

Guastello, S. J., Boeh, H., Shumaker, C., & Schimmels, M. (2012). Catastrophe models for cognitive workload and fatigue. Theoretical Issues in Ergonomics Science, 13(5), 586-602.

Guastello, S. J. (2014, September). Catastrophe Models for Cognitive Workload and Fatigue Memory Functions, Multitasking, Vigilance, Financial Decisions and Risk. In Proceedings of the Human Factors and Ergonomics Society Annual Meeting (Vol. 58, No. 1, pp. 904-908). SAGE Publications.

Guastello, S. J., Malon, M., Timm, P., Weinberger, K., Gorin, H., Fabisch, M., & Poston, K. (2014). Catastrophe models for cognitive workload and fatigue in a vigilance dual task. Human Factors: The Journal of the Human Factors and Ergonomics Society, 56(4), 737-751.

Guastello, S. J. (2016). Nonlinear dynamical systems for theory and research in ergonomics. Ergonomics, 1-27.

Guastello, S. J., Shircel, A., Malon, M., & Timm, P. (2015). Individual differences in the experience of cognitive workload. Theoretical Issues in Ergonomics Science, 16(1), 20-52.

Gundel, A., & Wilson, G. F. (1992). Topographical changes in the ongoing EEG related to the difficulty of mental tasks. Brain Topography, 5(1), 17-25.

Gutnichenko, O. A., Chen, L., Zhou, J. M., Bushlya, V. M., & Ståhl, J. E. (2014). Self-generated vibrations and process instability when turning high chromium white cast iron with PCBN tools. In 6th Swedish Production Symposium. The Swedish

Production Academy.

Hadjikhani, N., & Roland, P. E. (1998). Cross-modal transfer of information between the tactile and the visual representations in the human brain: a positron emission tomographic study. Journal of Neuroscience, 18(3), 1072-1084.

Hart, S. G., & Staveland, L. E. (1988). Development of NASA-TLX (Task Load Index): Results of empirical and theoretical research. In Advances in psychology (Vol. 52, pp. 139-183). North-Holland.

Heffernan, M. S. (1996). Comparative effects of microcurrent stimulation on EEG spectrum and correlation dimension. Integrative Psychological and Behavioral Science, 31(3), 202-209.

Hong, J., Li, X., Xu, F., Jiang, Y., & Li, X. (2012). The mental workload judgment in visual cognition under multitask meter scheme. International Journal of Physical Sciences, 7(5), 787-796.

Hou, X., Liu, Y., Sourina, O., & Mueller-Wittig, W. (2015, October). CogniMeter: EEG-based emotion, mental workload and stress visual monitoring. In Cyberworlds (CW), 2015 International Conference on (pp. 153-160). IEEE.

Humphrey, D. G., & Kramer, A. F. (1994). Toward a psychophysiological assessment of dynamic changes in mental workload. Human Factors, 36(1), 3-26.

Humphrey, D., Sirevaag, E., Kramer, A. F., & Mecklinger, A. (1990). Real-time measurement of mental workload using psychophysiological measures (No. NPRDC-TN-90-18). NAVY PERSONNEL RESEARCH AND DEVELOPMENTCENTER SAN DIEGO CA.

Iasemidis, L. D., & Sackellares, J. C. (1996). ■ REVIEW: Chaos Theory and Epilepsy. The Neuroscientist, 2(2), 118-126.

Kaber, D. B., Perry, C. M., Segall, N., & Sheik-Nainar, M. A. (2007). Workload state classification with automation during simulated air traffic control. The International Journal of Aviation Psychology, 17(4), 371-390.

Kannathal, N., Rjendra Acharya, U., Lim, C. M., & Sadasivan, P. K. (2005). Characterization of EEG - a comparative study. Computer Methods and Programs in Biomedicine, 80, 17-23.

Kanwisher, N., & Wojciulik, E. (2000). Visual attention: insights from brain imaging. Nature Reviews Neuroscience, 1(2), 91.

Kar, S., Bhagat, M., & Routray, A. (2010). EEG signal analysis for the assessment and quantification of driver's fatigue. Transportation Research Part F: Traffic Psychology and Behaviour, 13(5), 297-306.

Karwowski, W. (2000, July). Cognitive Ergonomics; Requisite Compatibility, Fuzziness and Nonlinear Dynamics. In Proceedings of the Human Factors and Ergonomics Society Annual Meeting (Vol. 44, No. 6, pp. 580-583). Sage CA: Los Angeles, CA: SAGE Publications.

Karwowski, W. (2005). Ergonomics and human factors: the paradigms for science, engineering, design, technology and management of human-compatible systems. Ergonomics, 48(5), 436-463.

Karwowski, W. (2012). A review of human factors challenges of complex adaptive systems: Discovering and understanding chaos in human performance. Human

factors, 54(6), 983-995.

Karwowski, W., Siemionow, W., & Gielo-Perczak, K., (2003). Physical Neuroergonomics: The Human Brain in Control of Physical Work Activities, Theoretical Issues in Ergonomics Science, 4 (1-2), 175-199.

Käthner, I., Wriessnegger, S. C., Müller-Putz, G. R., Kübler, A., & Halder, S. (2014). Effects of mental workload and fatigue on the P300, alpha and theta band power during operation of an ERP (P300) brain–computer interface. Biological psychology, 102, 118-129.

Kiehl, K. A., Laurens, K. R., Duty, T. L., Forster, B. B., & Liddle, P. F. (2001). Neural sources involved in auditory target detection and novelty processing: an event-related fMRI study. Psychophysiology, 38(1), 133-142.

Khushaba, R. N., Greenacre, L., Kodagoda, S., Louviere, J., Burke, S., & Dissanayake, G. (2012). Choice modeling and the brain: A study on the Electroencephalogram (EEG) of preferences. Expert Systems with Applications, 39(16), 12378-12388.

Khushaba, R. N., Wise, C., Kodagoda, S., Louviere, J., Kahn, B. E., & Townsend, C. (2013). Consumer neuroscience: Assessing the brain response to marketing stimuli using electroencephalogram (EEG) and eye tracking. Expert Systems with Applications, 40(9), 3803-3812.

Klingberg, T. (1998). Concurrent performance of two working memory tasks: potential mechanisms of interference. Cerebral cortex (New York, NY: 1991), 8(7), 593-601.

Klonowski, W., Ciszewski, J., Jernajczyk, W., & Niedzielska, K. (1999, November).

Application of chaos theory and fractal analysis for EEG-signal processing in patients with seasonal affective disorder. In Proceedings 1999 International Symposium on Nonlinear Theory and its Applications (NOLTA'99), Hawaii, USA (Vol. 1, pp. 339-342).

Kramer, A. F., Trejo, L. J., & Humphrey, D. (1995). Assessment of mental workload with task-irrelevant auditory probes. Biological Psychology, 40(1-2), 83-100.

Kriz, J. (2011). Chaos in the brain. Acta Physica Polonica A, 120, 6A, A-127-A-131.

Kriz, R. (2014). Finding chaos in Finnish GDP. International Journal of Automation and Computing, 11(3), 231-240.

Le, T. H., Pardo, J. V., & Hu, X. (1998). 4 T-fMRI study of nonspatial shifting of selective attention: cerebellar and parietal contributions. Journal of Neurophysiology, 79(3), 1535-1548.

Lei, S., & Roetting, M. (2011). Influence of task combination on EEG spectrum modulation for driver workload estimation. Human Factors: The Journal of the Human Factors and Ergonomics Society, 53(2), 168-179.

Lim, W. L., Sourina, O., Liu, Y., & Wang, L. (2015, December). EEG-based mental workload recognition related to multitasking. In Information, Communications and Signal Processing (ICICS), 2015 10th International Conference on(pp. 1-4). IEEE.

Litak, G., Syta, A., Budhraja, M., & Saha, L.M. (2009). Detection of the chaotic behaviour of a bouncing ball by the 0–1 test. Chaos, Solitons and Fractals, 42(3), 1511-1517.

Litak, G., Syta, A., & Wiercigroch, M. (2009). Identification of chaos in a cutting process by the 0-1 test. Chaos, Solitons and Fractals, 40(5), 2095-2101.

Liu, J., Zhang, C., & Zheng, C. (2010). EEG-based estimation of mental fatigue by using KPCA - HMM and complexity parameters. Biomedical Signal Processing and Control, 5(2), 124-130.

Lutzenberger, W., Birbaumer, N., Flor, H., Rockstroh, B., & Elbert, T. (1992). Dimensional analysis of the human EEG and intelligence. Neuroscience Letters, 143(1), 10-14.

Lutzenberger, W., Elbert, T., Birbaumer, N., Ray, W. J., & Schupp, H. (1992). The scalp distribution of the fractal dimension of the EEG and its variation with mental tasks. Brain Topography, 5(1), 27-34.

Macaluso, E., Frith, C., & Driver, J. (2000). Selective spatial attention in vision and touch: unimodal and multimodal mechanisms revealed by PET. Journal of Neurophysiology, 83(5), 3062-3075.

Mak, J. N., Chan, R. H., & Wong, S. W. (2013, November). Evaluation of mental workload in visual-motor task: Spectral analysis of single-channel frontal EEG. In Industrial Electronics Society, IECON 2013-39th Annual Conference of the IEEE (pp. 8426-8430). IEEE.

Matthews, G., Reinerman-Jones, L. E., Barber, D. J., & Abich IV, J. (2015). The psychometrics of mental workload: Multiple measures are sensitive but divergent. Human Factors, 57(1), 125-143.

Matthews, G., Reinerman-Jones, L., Wohleber, R., Lin, J., Mercado, J., & Abich, J.

(2015, August). Workload is multidimensional, not unitary: what now?. In International Conference on Augmented Cognition (pp. 44-55). Springer, Cham.

Matthews, G., Reinerman-Jones, L., Abich IV, J., & Kustubayeva, A. (2017). Metrics for individual differences in EEG response to cognitive workload: Optimizing performance prediction. Personality and Individual Differences, 118, 22-28.

Meyer-Lindenberg, A. (1996). The evolution of complexity in human brain development: an EEG study. Electroencephalography and clinical neurophysiology, 99(5), 405-411.

Miao, T., Oyama-Higa, M., Sato, S., Kojima, J., & Reika, S. (2012). Chaos of plethymogram in relation to scalp-EEG: A model and experiments. International Journal of Computer Aided Engineering and Technology, 4(6), 557-566.

Miller, M. W., Rietschel, J. C., McDonald, C. G., & Hatfield, B. D. (2011). A novel approach to the physiological measurement of mental workload. International Journal of Psychophysiology, 80(1), 75-78.

Miyake, S. (2001). Multivariate workload evaluation combining physiological and subjective measures. International Journal of Psychophysiology, 40(3), 233-238.

Murata, A., & Iwase, H. (1998). Analysis of chaotic dynamics in EEG and its application to assessment of mental workload. In Engineering in Medicine and Biology Society, 1998. Proceedings of the 20th Annual International Conference of the IEEE (Vol. 3, pp. 1579-1582). IEEE.

Natarajan, K., Acharya, R., Alias, F., Tiboleng, T., & Puthusserypady, S. K. (2004).

Nonlinear analysis of EEG signals at different mental states. BioMedical Engineering OnLine, 3(1), 7.

Navarro, J., & Arrieta, C. (2010). Chaos in human behavior: The case of work motivation. The Spanish Journal of Psychology, 13(01), 244-256.

Nobre, A. C., Gitelman, D. R., Dias, E. C., & Mesulam, M. M. (2000). Covert visual spatial orienting and saccades: overlapping neural systems. Neuroimage, 11(3), 210-216.

Nobre, A. C., Sebestyen, G. N., Gitelman, D. R., Mesulam, M. M., Frackowiak, R. S., & Frith, C. D. (1997). Functional localization of the system for visuospatial attention using positron emission tomography. Brain: a journal of neurology, 120(3), 515-533.

Pardo, J. V., Fox, P. T., & Raichle, M. E. (1991). Localization of a human system for sustained attention by positron emission tomography. Nature, 349(6304), 61.

Patten, C. J. (2007). Cognitive workload and the driver: Understanding the effects of cognitive workload on driving from a human information processing perspective (Doctoral dissertation, Psykologiska institutionen).

Preißl, H., Lutzenberger, W., Pulvermüller, F., & Birbaumer, N. (1997). Fractal dimensions of short EEG time series in humans. Neuroscience Letters, 225(2), 77-80.

Pritchard, W. S., & Duke, D. W. (1992). Measuring chaos in the brain: a tutorial review of nonlinear dynamical EEG analysis. International Journal of Neuroscience, 67(1-4), 31-80.

Quiroga, R. Q. (1998). Quantitative analysis of EEG signals: time-frequency methods and chaos theory (Doctoral dissertation). Institute of Physiology-Medical University Lubeck and Institute of Signal Processing-Medical University Lubeck.

Rabbi, A. F., Ivanca, K., Putnam, A. V., Musa, A., Thaden, C. B., & Fazel-Rezai, R. (2009, September). Human performance evaluation based on EEG signal analysis: a prospective review. In Engineering in Medicine and Biology Society, 2009. EMBC 2009. Annual International Conference of the IEEE(pp. 1879-1882). IEEE.

Reinerman-Jones, L. E., Matthews, G., Barber, D. J., & Abich IV, J. (2014, September). Psychophysiological metrics for workload are demand-sensitive but multifactorial. In Proceedings of the Human Factors and Ergonomics Society Annual Meeting (Vol. 58, No. 1, pp. 974-978). Sage CA: Los Angeles, CA: Sage Publications.

Rodrick, D., & Karwowski, W. (2006). Nonlinear dynamical behavior of surface electromyographical signals of biceps muscle under two simulated static work postures. Nonlinear dynamics, psychology, and life sciences,10(1), 21-35.

Rouse, W. B., Edwards, S. L., & Hammer, J. M. (1993). Modeling the dynamics of mental workload and human performance in complex systems.IEEE transactions on systems, man, and cybernetics, 23(6), 1662-1671.

Sammer, G., Blecker, C., Gebhardt, H., Bischoff, M., Stark, R., Morgen, K., & Vaitl, D. (2007). Relationship between regional hemodynamic activity and simultaneously recorded EEG□theta associated with mental arithmetic□induced

workload. Human brain mapping, 28(8), 793-803.

Shulman, G. L., Ollinger, J. M., Akbudak, E., Conturo, T. E., Snyder, A. Z., Petersen, S. E., & Corbetta, M. (1999). Areas involved in encoding and applying directional expectations to moving objects. Journal of Neuroscience, 19(21), 9480-9496.

Sirevaag, E. J., Kramer, A. F., REISWEBER, C. D. W. M., STRAYER, D. L., & GRENELL, J. F. (1993). Assessment of pilot performance and mental workload in rotary wing aircraft. Ergonomics, 36(9), 1121-1140.

Son, J., Mehler, B., Lee, T., Park, Y., Coughlin, J. F., & Reimer, B. (2011, June). Impact of cognitive workload on physiological arousal and performance in younger and older drivers. In Proceedings of the Sixth International Driving Symposium on Human Factors in Driver Assessment, Training, and Vehicle Design, Lake Tahoe, CA (pp. 87-94).

Stam, C. J. (2005). Nonlinear dynamical analysis of EEG and MEG: review of an emerging field. Clinical neurophysiology, 116(10), 2266-2301.

Sterman, J. D. (1988). Deterministic chaos in models of human behavior: Methodological issues and experimental results. System Dynamics Review,4(1‐2), 148-178.

Sun, K., Liu, X., & Zhu, C. (2010). The 0-1 test algorithm for chaos and its applications. Chinese Physics B, 19(11), 110510-1-110510-7.

Taylor, G., Reinerman-Jones, L., Cosenzo, K., & Nicholson, D. (2010, September). Comparison of multiple physiological sensors to classify operator state in adaptive automation systems. In Proceedings of the Human Factors and

Ergonomics Society Annual Meeting (Vol. 54, No. 3, pp. 195-199). Sage CA: Los Angeles, CA: Sage Publications.

Takens, F. (1981). Detecting strange attractors in turbulence. In Dynamical systems and turbulence, Warwick 1980 (pp. 366-381). Springer Berlin Heidelberg.

Teo, G., Reinerman-Jones, L., Matthews, G., Szalma, J., Jentsch, F., & Hancock, P. (2018). Enhancing the effectiveness of human-robot teaming with a closed-loop system. Applied ergonomics, 67, 91-103.

Teo, G., Reinerman-Jones, L., Matthews, G., & Szalma, J. (2015). Comparison of measures used to assess the workload of monitoring an unmanned system in a simulation mission. Procedia Manufacturing, 3, 1006-1013.

Teo, G., Reinerman-Jones, L., Matthews, G., Szalma, J., Jentsch, F., Hudson, I., & Hancock, P. A. (2017, September). Selecting Workload and Stress Measures for Performance Prediction. In Proceedings of the Human Factors and Ergonomics Society Annual Meeting (Vol. 61, No. 1, pp. 2042-2046). Sage CA: Los Angeles, CA: SAGE Publications.

Trejo, L. J., Knuth, K., Prado, R., Rosipal, R., Kubitz, K., Kochavi, R., ... & Zhang, Y. (2007, July). EEG-based estimation of mental fatigue: convergent evidence for a three-state model. In International Conference on Foundations of Augmented Cognition (pp. 201-211). Springer, Berlin, Heidelberg.

Tumey, D. M., Morton, P. E., Ingle, D. F., Downey, C. W., & Schnurer, J. H. (1991, April). Neural network classification of EEG using chaotic preprocessing and phase space reconstruction. In Bioengineering Conference, 1991., Proceedings of

the 1991 IEEE Seventeenth Annual Northeast (pp. 51-52). IEEE.

Tzourio, N., El Massioui, F., Crivello, F., Joliot, M., Renault, B., & Mazoyer, B. (1997). Functional anatomy of human auditory attention studied with PET. Neuroimage, 5(1), 63-77.

Ullsperger, Peter, Gabriele Freude, and Udo Erdmann. "Auditory probe sensitivity to mental workload changes–an event-related potential study." International Journal of Psychophysiology 40.3 (2001): 201-209.

Webel, K. (2012). Chaos in German stock returns - New evidence from the 0-1 test. Economics Letters, 115(3), 487–489.

Wilson, G. F. (2002). An analysis of mental workload in pilots during flight using multiple psychophysiological measures. The International Journal of Aviation Psychology, 12(1), 3-18.

Wolf, A., Swift, J. B., Swinney, H. L., & Vastano, J. A. (1985). Determining Lyapunov exponents from a time series. Physica D: Nonlinear Phenomena,16(3), 285-317.

Xingyuan, W., & Chao, L. (2006). Researches on chaos phenomenon of EEG dynamics model. Applied Mathematics and Computation, 183(1), 30-41.

Xu, J., Wang, H., & Fang, H. (2011). Characterization of periodic, quasiperiodic, and chaotic states in nonpremixed biodiesel/air jet flames. Mathematical Problems in Engineering, 2011.

Yin, Z., & Zhang, J. (2014). Identification of temporal variations in mental workload using locally-linear-embedding-based EEG feature reduction and support-vector-machine-based clustering and classification techniques. Computer methods and

programs in biomedicine, 115(3), 119-134.

Yuasa, M., & Saha, L. M. (2008). Indicators of chaos, Science and Technology, 20, 1-12.

Zarjam, P., Epps, J., Chen, F., & Lovell, N. H. (2013). Estimating cognitive workload using wavelet entropy-based features during an arithmetic task.Computers in biology and medicine, 43(12), 2186-2195.

Zarjam, P., Epps, J., Lovell, N. H., & Chen, F. (2012, August). Characterization of memory load in an arithmetic task using non-linear analysis of EEG signals. In Engineering in Medicine and Biology Society (EMBC), 2012 Annual International Conference of the IEEE (pp. 3519-3522). IEEE.